

Czech Technical University  
Department of Control engineering

**SpaceMaster program**



# In-situ wear process monitoring by optical methods

Diploma thesis

Supervisor:

doc. Ing.Tomas Polcar.Ph.D.

Author:

Michal Kostyál

Prague, 2012



Name of the author:	Michal Kostyál
Thesis Title:	In-situ wear process monitoring by optical methods
Department:	Department of Control Engineering
Supervisor:	doc. Ing.Tomas Polcar.Ph.D.
Year of defense:	2012

## **Abstract**

The thesis describes the development of methodology for in-situ observation of a wear process. The main goal is to correlate the friction coefficient development with the video record. It is approached by designing the external device that counts the cycles and determines the period based on infrared reflectance sensor. Another problem solved is the evaluation of the possibility of using the external probe for the in-situ Raman spectra measurement. The proposed interpretation technique is used for the deviation measurement at different rotational velocities. The techniques are demonstrated on the steel samples and DLC samples.



Czech Technical University in Prague  
Faculty of Electrical Engineering

Department of Control Engineering

## DIPLOMA THESIS ASSIGNMENT

Student: **Michal Kostyal**

Study programme: Cybernetics and Robotics  
Specialisation: Systems and Control

Title of Diploma Thesis: **In-situ wear process monitoring by optical methods**

### Guidelines:

Solid lubricant coatings are widely used to decrease sliding friction of mechanisms operating in aero-space application. Transition metal dichalcogenides (TMDs) are established solid lubricant coatings for vacuum, whereas diamond-like carbon (DLC) is an excellent coating for humid air. The friction is typical the only parameter measured during the sliding process. We will add optical methods (microscope, Raman) to identify changes of surface morphology and chemistry.

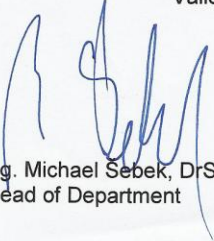
The main goal of the thesis is to develop the method of in-situ optical wear measurement; the method will be tested on TMD alloyed with carbon and DLC coatings and compared with standard ex situ measurements. The core objective is to relate friction coefficient with surface morphological and structural changes observed by optical microscope and Raman spectroscopy.

### Bibliography/Sources:

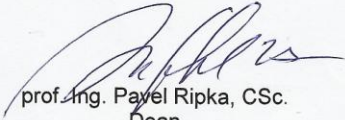
Will be provided by the supervisor

Diploma Thesis Supervisor: doc. Ing. Tomáš Polcar, Ph.D.

Valid until the summer semester 2012/2013

  
prof. Ing. Michael Sebek, DrSc.  
Head of Department



  
prof. Ing. Pavel Ripka, CSc.  
Dean

Prague, January 17, 2012



## Acknowledgement

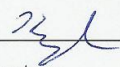
I would like to thank doc. Ing.Tomas Polcar.Ph.D., who was very kindly guiding and supporting me with his knowledge. I would also like to thank Ing. Joao Vitor Pimentel Bernardo and Ing. Jaroslav Žoha for their support.



Proclamation

I honestly claim that I have done my Diploma thesis all by myself and I have used only the materials (literature, projects, SW etc.) stated in the attached list.

In Prague May 15th 2012

  
\_\_\_\_\_  
Signature



## Table of content

Introduction .....	3
1. Tribology.....	5
1.1. Friction .....	6
1.1.1. Friction of solids .....	6
1.1.2. Friction measurement.....	7
1.2. Wear.....	9
1.2.1. Adhesion.....	9
1.2.2. Abrasive wear.....	10
1.2.3. Surface fatigue, erosion, corrosion .....	11
1.3. Lubrication .....	12
1.4. Lubricants.....	14
1.4.1. Lubricating oils .....	14
1.4.2. Lubricating Greases .....	14
1.4.3. Solid lubricants .....	15
1.5. Diamond Like Carbon.....	17
1.5.1. Application of DLC coatings .....	19
2. Methodological part.....	21
2.1. Problem description.....	21
2.2. Instruments description.....	23
2.2.1. Tribometer .....	23
2.2.2. Profilometer .....	24
2.2.3. Raman Microscope.....	25
2.2.4. External objective.....	26
2.3. Raman spectroscopy.....	27
2.3.1. Raman spectra interpretation of DLC .....	28
2.4. Raman spectra measurement.....	29
2.4.1. Raman spectra comparison.....	30
2.4.2. Raman spectra of rotating sample.....	31
2.5. Video recording optimization .....	34
2.5.1. Sensor design .....	35
2.5.2. Video recording.....	38

2.5.3. Testing the tribometer rotation.....	38
2.5.4. Initial period .....	40
2.6. Ex-situ wear track profile measurement .....	41
3. Measurements .....	42
3.1. Algorithm of the measurements .....	42
3.2. Tribological tests using steel samples .....	44
3.3. Future work .....	49
Conclusion.....	50
References .....	52
Tables .....	58
Figures.....	58
List of Appendices.....	60

## Introduction

One of the most important life-limiting problems of the aerospace systems is friction and wear (1). As the space environment requires the functionality under very severe conditions, conventional lubricants often fail to provide sufficient lubrication. In contrary, coating of solid lubricants can reduce friction between the surfaces without the need for a liquid media. Currently metal dichalcogenides such as molybdenum disulphide ( $\text{MoS}_2$ ) are established solid lubricants (2). Diamond-like carbon (DLC) is an emerging coating that has shown promising tribological characteristics and is currently being explored also in the field of space technology (3).

To understand the sliding process and different acting wear mechanisms, various optical methods such as Raman spectrometry, optical camera 3D surface metrology are used. However, typical analysis of the worn surfaces is carried out after the test. It is very difficult then (or even impossible) to trace all possible changes on the worn surface in time. To remedy this lack, in-situ observation could be applied.

The main goal of the thesis is to develop a method of in-situ optical wear measurement and correlate it with a friction coefficient measurement. In addition the wear will be tested employing ex-situ methods such as 3D surface metrology. The method will be tested on various samples.

The aim is also to compare the composition evaluation of in-situ and ex-situ measurements using Raman spectroscopy. This will be tested for various speed of rotation.

In the theoretical introduction will be a short summary of tribology. Special attention will be given to DLC as an emerging coating for space industry. That will be followed by references to similar measurements as well as instruments description. Focus will be given to devices which were developed in the author's laboratory.

In the rest of the work, the author will approach the problem designing a methodology of in-situ measurement, as described above. The methodology will be tested mainly on DLC samples. On each method, used in the methodology, the author will evaluate its inaccuracy.

The methodology will be demonstrated on a few measurements of the wear process on various samples. The surface morphology will be studied using in-situ methodology. The results will be compared and correlated with ex-situ methods.

# 1. Tribology

„It is quite difficult to do accurate quantitative experiments in friction, and the laws of friction are still not analyzed very well, in spite of the enormous engineering value of an accurate analysis “

(Richard P. Feynman, Nobel laureate, 1963)

Tribology (derived from Greek *tribos* – rubbing, sliding) was first defined in 1966 as science and engineering of interacting surfaces in relative motion (4). It is technical application-oriented multidisciplinary area, which studies the principles of friction, lubrication and wear.

Czichos recognizes three main utilizations of the Tribology (5):

## 1. Scientific

Tribology as a science describes forces and mechanisms which occur during interaction of surfaces in relative motion leading to dissipation of energy and material (6).

## 2. Multidisciplinary

Tribology is widely recognized as a branch of Mechanical engineering. It utilizes results from research of surface science, mechanics, material science and other disciplines to study and modify the surfaces (7).

## 3. Economic

The surface interaction leading to surface degradation and material loss occurs on virtually every mechanical device as well it has enormous influence on various industries and the economy as a whole. Some studies estimate that in highly industrialized countries the tribology-related losses account to about 4% of the Gross domestic product (8).

The core objective of the tribological studies is to optimize friction and wear (typically with the lowest possible manufacturing and maintenance costs), for the given application (9).

## 1.1. Friction

Friction is a force counteracting relative motion of the bodies' material zones that are in a contact. It is denoted as internal, for material zones belonging to different friction bodies, or external, for material zones belonging to one of the friction body (9).

### 1.1.1. Friction of solids

The friction can appear in three states of material zones involved: Solid, Gas, Fluid (10).

Solid friction is interaction of the elements which exhibit solid properties. If the body surfaces are completely separated by a lubricant film, it is described as a fluid friction (see chapter 1.3).

Based on relative movement of the bodies, solid friction is further classified as static or dynamic friction (11). While dynamic (kinetic) friction occurs between two objects in relative movement, static friction is between bodies that do not move relatively. The maximum force before the sliding begins is called static friction force, while the kinetic friction force needs to be applied to continue the sliding process. For majority of materials the static friction is higher than kinetic one; stick-slip mechanism (12) is typical demonstration of difference between these two phenomena.

According to the type of relative motion we can distinguish two types of solid friction (13):

- Rolling
- Sliding

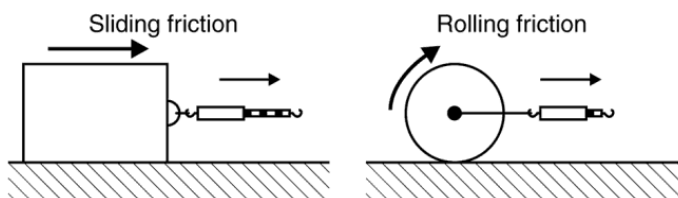


**Figure 1 Types of friction (13)**

Friction is normally expressed in a form of the friction coefficient  $\mu$ , which is the ratio of the friction force  $F_f$  to the normal force  $F_n$  :

$$\mu = \frac{F_f}{F_n} . \quad [1]$$

### 1.1.2. Friction measurement

Surface friction is normally measured using tribometer. Additional information about the surface (such as roughness and structure) can be obtained using various optical methods (see chapter 2.2).

Tribometers may employ several mechanisms. We can distinguish pin on disc tribometer, four ball tribometer, ball on plate tribometer and many others.

The pin on disc tribometer determines the magnitude of friction as two surfaces rub together. The end of the pin can have any shape but spherical tips are preferred due to contact geometry (14). The probe is loaded using passive (dead load) or active systems. The sample is rotating and the resulting frictional forces acting between the pin and the sample are measured (15). This is made by measuring the deflection of the lever (elastic arm) attached to the probe (see Figure 2).

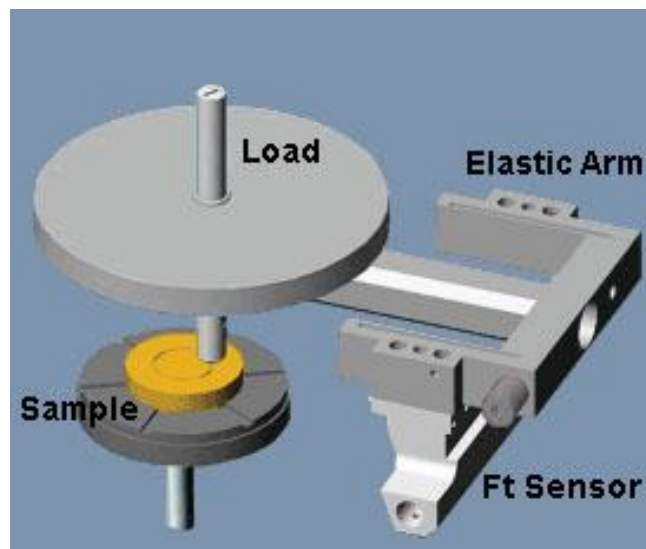
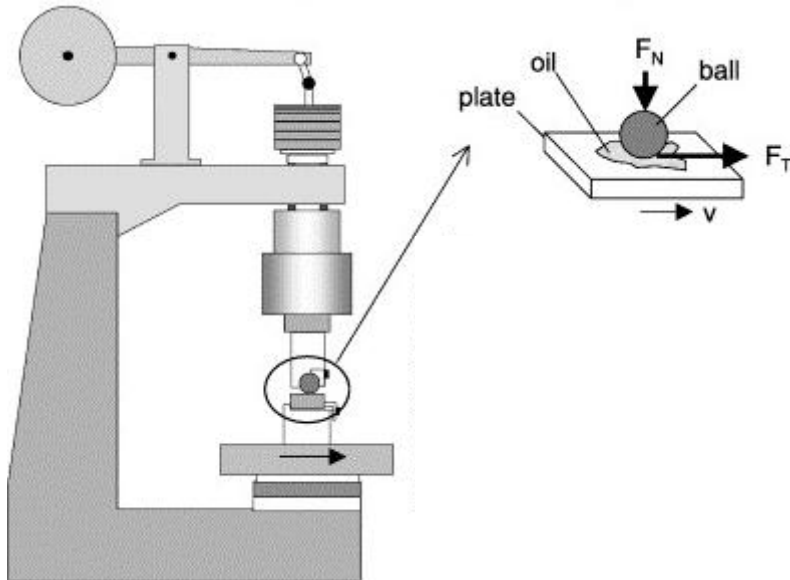


Figure 2 Tribometer (15)

Ball on plate tribometer is used to quantify static friction and the transition from static to kinetic friction. The principle is similar to the pin on disc tribometer, but the sample is not rotating, see Figure 3.



**Figure 3** Example of ball on plate tribometer (58)

The four-ball wear machine is used to measure anti-wear properties of lubricating oils. Three fixed balls (in Locking ring) are positioned against rotating ball attached to Ball chuck with a load. The frictional torque exerted on the three lower balls is measured by a calibrated arm (59).

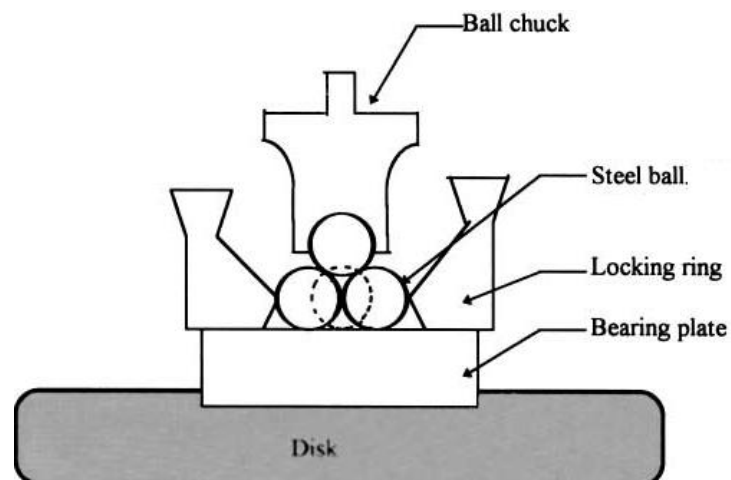


**Figure 4** Four-ball tribometer (59)

## 1.2.Wear

The interaction between surfaces may lead to a displacement of material. Wear is defined as a progressive loss of material from the surface of a solid body due to the contact or frictional motion against counter-body (solid, fluid, gaseous) (16).

Wear is the result of different mechanisms (17):

- Abrasive wear
- Adhesive wear
- Surface fatigue, erosion, tribo-corrosion

### 1.2.1. Adhesion

Adhesion wear leads to high wear rates, large and unstable friction coefficient. Sliding contact can be destroyed entirely (18). Adhesion is significant predominantly among metals. The reason behind this is electron bonding, which can arise for small distances between surfaces of two bodies. This allows electrons to move between surfaces and the bonding force can arise (19) .

It occurs particularly when surfaces are not separated by atmospheric contaminants. Lubricants are also successfully used to separate surfaces avoiding adhesion (20).

The Figure 5 schematically shows the adhesive wear between stronger and weaker material.

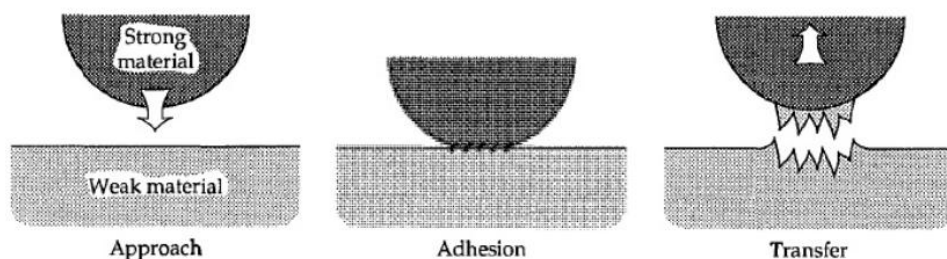


**Figure 5 Mechanism of Adhesion (18)**

### 1.2.2. Abrasive wear

Abrasive wear is the loss of material by passage of hard particles over a surface. It occurs when a solid object is loaded against particles of material with greater hardness.

Four mechanisms of abrasive wear can be distinguished (21):

a) Cutting

Softer surface is altered by a sharp grid and removed as debris.

b) Fracture

Crack caused by convergence in the brittle materials.

c) Fatigue

Surface deformation caused by repeated strain often by a blunt grit.

d) Grain detachment

In the material with weak boundaries between grains the entire grain can be pull out.

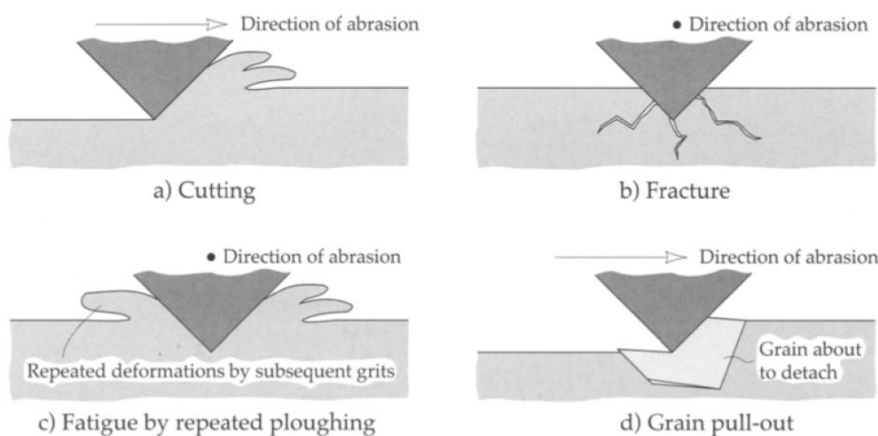


**Figure 6 Mechanism of Abrasive wear (18)**

There are two basic modes of Abrasive wear (22):

In two body mode, hard grits attached to one of the surfaces pass over the other surface. In three body mode, grits are moving freely between the surfaces.

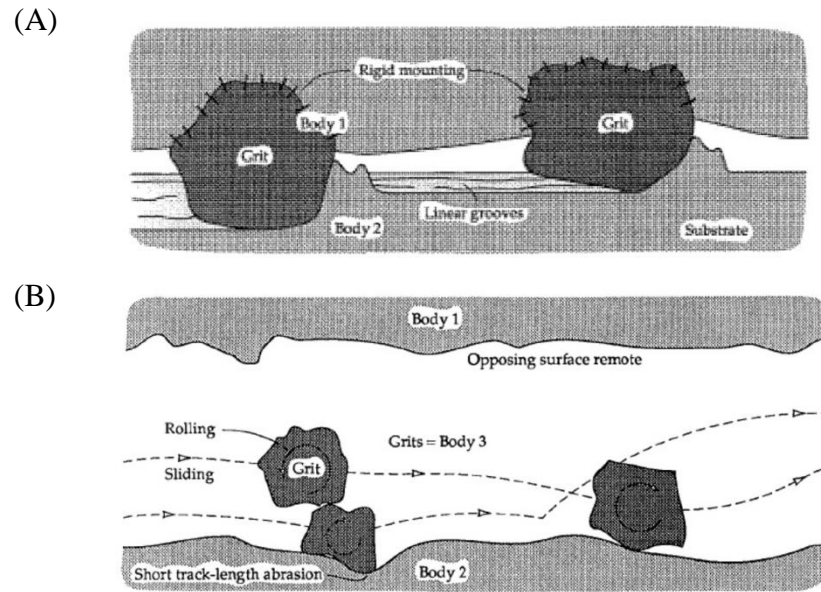


**Figure 7 Modes of Abrasive wear (18)**

### **1.2.3. Surface fatigue, erosion, corrosion**

The surface fatigue is caused by repeated stress cycling (loading, unloading). It leads to a localized structural damage. It manifests itself through microscopic cracking of the surface (23).

Erosive wear is caused by an impact of relatively small particles against a solid surface. The impact depends on particle's velocity, size, hardness as well as an angle between its trajectory and the eroded surface (9).

Corrosive wear is caused by chemical reaction of a surface mainly with atmospheric oxygen.

### 1.3.Lubrication

Lubrication completely or partially separates the surface of solid friction bodies. It improves the smoothness of movement of one surface over another, lowers the friction and prevents the damage (24).

By level of separation of the friction partners and magnitude of the friction coefficient, four states of friction (and lubrication) can be distinguished (9):

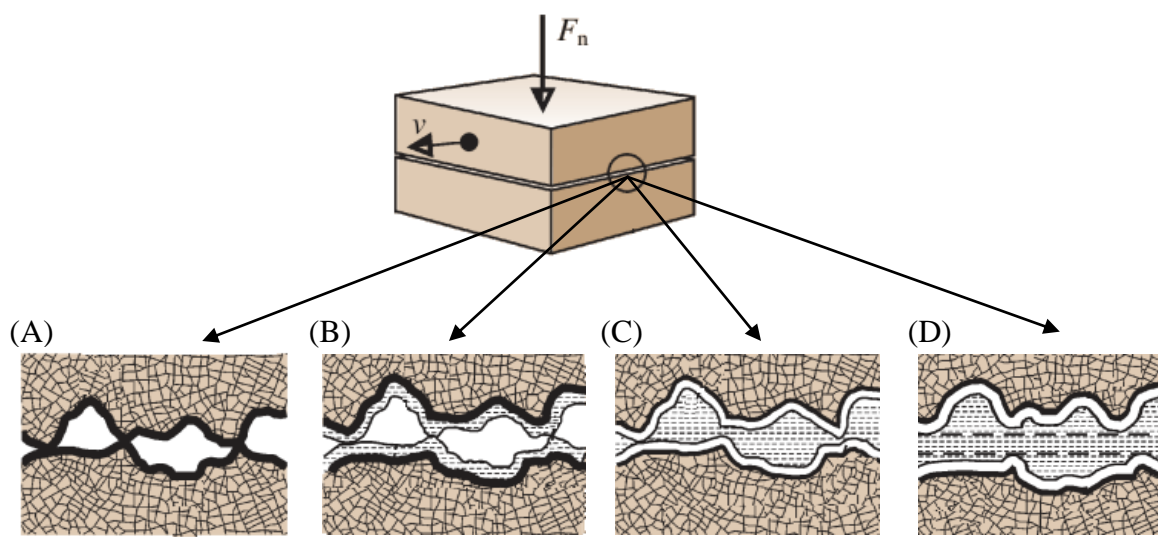


**Figure 8 States of friction (9)**

A) Solid friction, (B) Boundary lubrication, (C) Mixed lubrication, (D) Fluid lubrication

Solid friction is characterized by direct contact of the friction partners and high friction coefficients (0.35 – 1). No lubrication is present (see also chapter 1.1.1).

In Boundary lubrication, the friction partners are covered though not separated by a thin lubrication film (25). The friction is influenced by properties of contact surfaces rather than properties of a lubricant. The friction coefficient, reaching 0.06 – 0.2, is independent of lubricant's viscosity. Between the surfaces are formed boundary layers with the thickness of about 1 – 10 nm, the property of which is given mainly by lubricant additives (9).

Fluid lubrication is characterized by complete separation of the friction partners and very low friction coefficient ( $6 \times 10^{-4}$  -  $5 \times 10^{-3}$ ).

Fluid lubrication can be achieved by two mechanisms (18) :

- Hydrodynamic lubrication arises when two surfaces move relatively to each other with sufficient velocity and relative angle (26). As illustrated on Figure 9, this generates hydrodynamic pressure, which separates the surfaces and can support a load.
- In Hydrostatic lubrication, the separation of bearing surfaces is achieved by external pressure, normally generated by pump. The film thickness, often as high as 100  $\mu\text{m}$ , prevents contact between surfaces even at zero sliding speed.

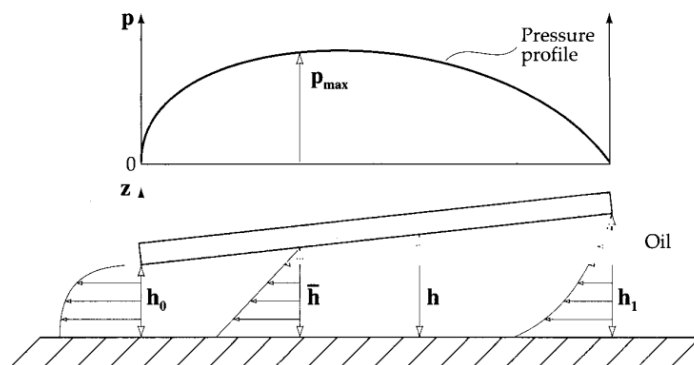


**Figure 9 Principle of hydrodynamic lubrication (18)**

In Mixed lubrication, the contact between hydrodynamically lubricated elements appears in some points. The film is no more coherent, which leads to coexistence of fluid friction with boundary friction, with the friction coefficient reaching approximately  $10^{-3} - 10^{-1}$  (27).

The regimes of lubrication are often depicted in what is called a Stribeck curve. The velocity of the surfaces in relative motion determines the thickness of the fluid film, which in turn affects a friction coefficient and a lubrication regime. The simplified Stribeck curve is shown on Figure 10.

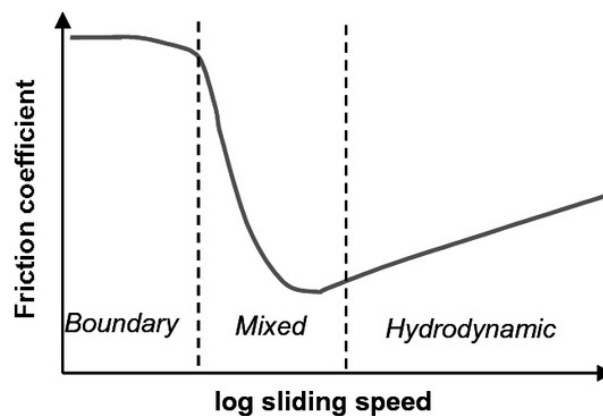


**Figure 10 Stribeck curve (simplified) (54)**

## **1.4.Lubricants**

Lubricants are gaseous, liquid or solid films with a thickness of about 1 – 100  $\mu\text{m}$ . Gaseous lubricants are used in high-speed, low loaded machines; fluid lubricants include natural and synthetic oils; greases are consistent lubricants; solid lubricants can be used under conditions, where others fail (9).

### **1.4.1. Lubricating oils**

Mineral oils are obtained from naturally deposited crude oil; desired composition and properties are achieved by specific manufacturing process. Due to oxidation, mineral oils exhibit gradually diminishing performance (28).

Synthetic oils, produced by chemical synthesis, are designed to satisfy extreme requirements. They may have three to five times better resistance to aging, and lower sensibility to temperature (9). Synthetic oils, however, cannot be used universally as they are often toxic. Moreover the price might be considerably higher compared to mineral oils.

The properties of lubricating oils can be altered significantly using additives (29). They can improve heat dissipation, temperature resistance, aging stability, or offer protection against corrosion.

### **1.4.2. Lubricating Greases**

Unlike lubricating oils, Greases do not provide cooling and cleaning functions. On the other hand they can better resist contamination and the washing action of water. According to Exxon, Greases are uniquely suited especially in applications where relubrication is not frequent (30).

Lubricating Greases consist of (31):

- Base oil, accounting for 80-96%, can be any fluid providing lubricating properties (normally lubrication oil).
- Thickener, in combination with the base oil, producing the solid to semi-fluid structure. Most commonly used are lithium, aluminum or calcium soaps.
- Additives, modifying performance characteristics.

Due to lower maximum operational temperature ( $\approx 350^\circ\text{C}$ ) they are mostly used at low speeds.

### 1.4.3. Solid lubricants

Solid lubricants are used particularly at low sliding speed, high specific load, extreme temperature, or pressure (vacuum), radioactive environment, or whenever oils and greases cannot provide sufficient lubrication (32).

Two most important types of solid lubricants are substances with lamellar structure (e.g. graphite, molybdenum disulphide) and soft metals (e.g. silver, gold). Solid lubricants are often, applied as thin films due to technological and economic reasons.

Even a thin film of soft metal on a hard substrate can considerably decrease shear strength, while only the hard surface determines the contact area (as shown on Figure 11). This leads to decrease of friction force, which is given by (33):

$$F = A \cdot \tau, \quad [2]$$

where  $A$  is contact area and,  $\tau$  is shear strength of weaker metal.

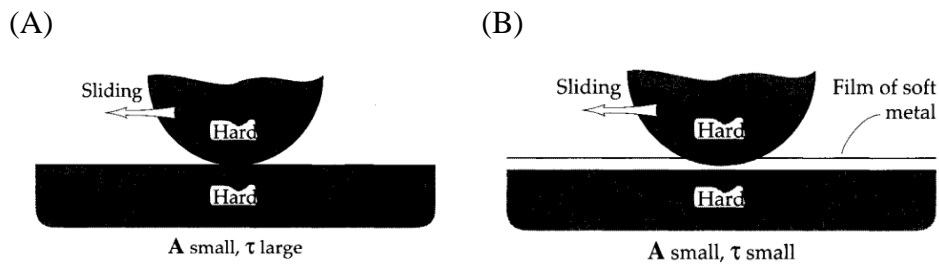


**Figure 11 Friction reduction by soft metal film (18)**

(A) Without the soft metal film, (B) with soft metal coating.

Lamellar solids exhibit anisotropy of mechanical properties and friction (34). The solid lubricants are often termed as self-lubricants, since the lamellas are able, at low shear stress, to slide one over another, while adhering strongly to the worn surface.

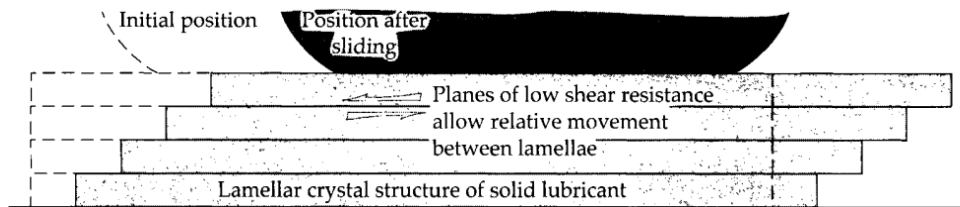


**Figure 12 Lubrication by lamellar solids (18)**

For lamellar solids are characteristic strong chemical bonds between atoms on planes (lamellas) and weak, usually Van der Waals bonding, between lamellas (see Figure 13). The most known and used are graphite and Molybdenum disulphide ( $\text{MoS}_2$ ).

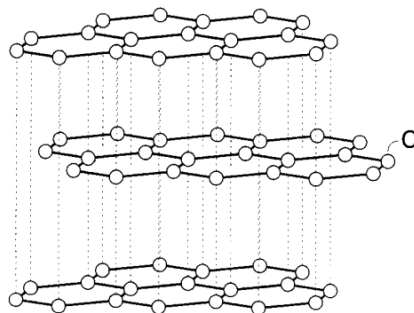


**Figure 13 Structure of graphite (25)**

Load and sliding speed limit lifetime of the lamellar solids, rather than influence friction coefficient, Molybdenum disulphide being considerably less sensible to both of them (in compare to graphite). However,  $\text{MoS}_2$  is sensitive to air humidity and its use is limited mainly to dry and vacuum conditions (35). On the other hand, graphite requires humid air to achieve low friction.

## 1.5. Diamond Like Carbon

Diamond Like Carbon (DLC) has shown exceptional optical, electrical as well as mechanical properties. Low friction and extremely high hardness make it an excellent tribological coating. Moreover it is resistant to corrosive and oxidative attacks and biocompatible (36).

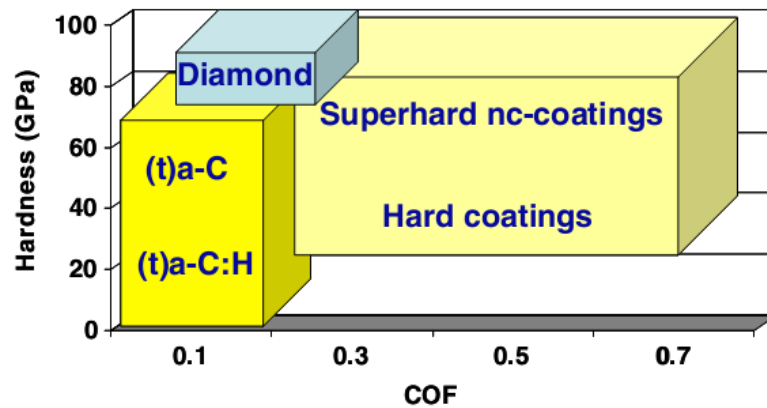


**Figure 14 Hardness and friction characteristics of DLC (9)**

(t)a-C and (t)a-C:H are two forms of DLC; COF states for coefficient of friction.

DLC films are structurally amorphous (37). They are made of carbon atoms with  $sp^2$  and  $sp^3$  bonds often with some amount of hydrogen. Depending of the  $sp^2$  and  $sp^3$  bonds ratio and the amount of hydrogen we can distinguish many different forms of DLC as shown on Figure 15.

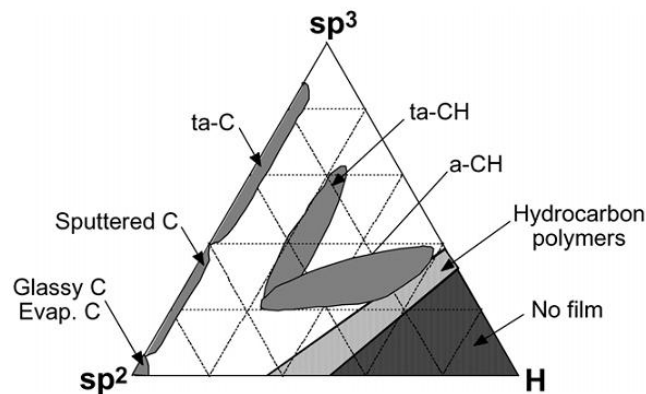


**Figure 15 Phase diagram of the DLC (40)**

DLC coatings differ in structure (such as  $sp^3$  bonds ratio) as well as resulting properties such as hardness. The comparison of the properties of three DLC forms (a-C:H, ta-C, a-C) with various carbon materials is shown on Table 1.

Material	Form	Density (g/cm <sup>3</sup> )	Covalent bonds	Young's modulus (GPa)	Hardness (GPa)	Tensile strength (GPa)
C60	Films	~1.7	Almost all $sp^2$	?	~0.2	–
C fibres	Fibres	1.7–1.9	Almost all $sp^2$	200–600	?	3.8–6.4
Graphite	Bulk	~2	100% $sp^2$	10	0.2–2	–
CNT	Fibres	~2	Almost all $sp^2$	1000	?	1
CNT	Film	<2?	Almost all $sp^2$	0.013	?	–
FLC	Films	~2.2	Almost all $sp^2$	480	45	–
a-C	Films	~2.2	$sp^2$ -rich	100–200	10–20	–
a-C:H	Films	~2.2	Intermediate $sp^3$	100–300	10–30	–
t-aC	Films	3–3.2	$sp^3$ -rich	300–500	50–80	–
Diamond	Bulk, films	~3.5	100% $sp^3$	1000	100	–

**Table 1 Comparison of mechanical properties of DLC with various carbon materials (51)**

t-aC, a-C, a-C:H are different forms of DLC

DLC coating provide not only low friction but also high wear resistance. The friction coefficient generally ranges from 0.2 to 0.05. However, it can reach as low as 0.01 (or even lower), which is sometimes termed as superlubricity (20). Low friction means lower loss of energy and higher reliability.

At the same time some forms of DLC (such as ta-C) can have hardness of 80 GPa, higher than most metals. It gives the coating very high wear resistance.

Thanks to the properties, it affords high efficiency and durability in sliding mechanisms.

DLC coating can be deposited on various substrates; however the adhesion improving interlayer (metallic such as Ti or Cr, or gradient layer) is often applied between the substrate and top functional DLC film (38).

There are various methods to deposit DLC coating with different structural, mechanical and tribological properties. Chemical vapor deposition (CVD) and Physical vapor deposition (PVD) are routinely used for hydrogenated DLC film production. To add hydrogen, hydrogen-containing gas (methane, ethylene) is introduced into the chamber during the deposition (39).

DLC films are often referred as metastable materials as their structure changes by thermal activation or irradiation of energetic photons towards graphite-like carbon. The process starts at about 400°C and may result in a loss of hydrogen (40). For hydrogenated DLC (a-C:H). This may significantly increase the friction coefficient as demonstrated on Figure 16. Similar process happens during sliding.

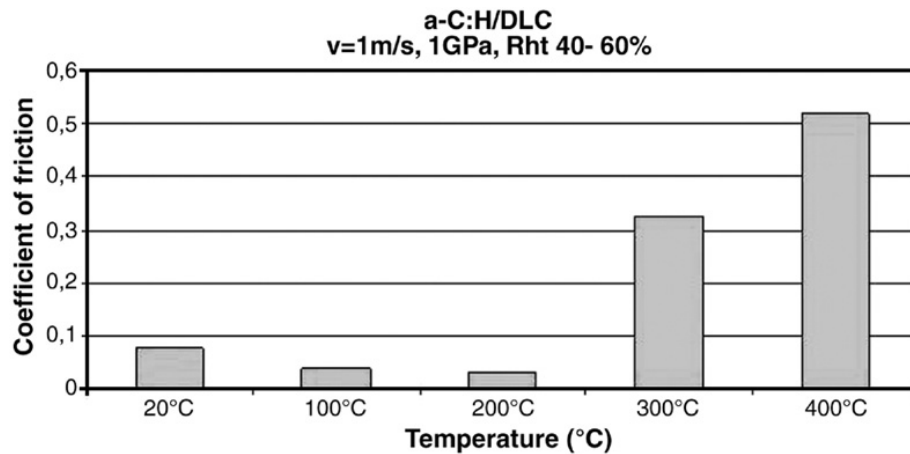


**Figure 16 Influence of temperature on friction coefficient (55)**

DLC coatings may be doped with different metals such as Ti, Nb, Ta, Cr and many others, to change their mechanical and tribological properties.

### **1.5.1. Application of DLC coatings**

Thanks to extraordinary properties referred to above, DLC coating has been investigated in last decade and applied in numerous industrial applications. They include razor blades, magnetic hard discs, critical engine parts, medical devices, scratch-resistant glasses, microelectromechanical systems and many others (36).

As a lubricant it is used particularly when conventional lubricants cannot provide sufficient lubrication due to operating conditions, or when it is not possible to use them (e.g. due to cleanness). It meets to very high extend the demands of the space environment such as wide operating temperature range, absence of gravity, lack of oxygen and presence of radiation (2).

The problem may arise in a presence of ultra-high vacuum. The adhesion or even cold-welding between non/low hydrogenated DLC film and counterpart often occurs (3). This is often attributed to high surface energy of the DLC film.

Higher content of hydrogen in DLC (as much as 60%) can significantly decrease the surface energy and resulting adhesion. In fact highly hydrogenated DLC has usually extremely low friction coefficient in a vacuum (41). However this decreases the Young module about three folds (40). Liquid lubricants are likewise successfully used to avoid adhesion.

DLC films show consistency of friction in ambient atmosphere. This is important when the assembly, test and storage phases are not carried out in vacuum (42).

Although DLC coatings are getting more and more used in practice, there is still lack of knowledge about properties and tribological behavior (43).

## 2. Methodological part

### 2.1. Problem description

As described in the introduction (on page 3) a lot of valuable information about the wear mechanism can be acquired from in-situ observation. However, the in-situ experiments require specific instruments and algorithms and only few research groups have implemented these new techniques. In fact, by author's knowledge, only one research group focused on solid lubricants carried out experiment similar to one which will be described in the thesis.

In situ Raman tribometry of DLC was performed by Singer and Scharf from U.S. Naval Research Laboratory. The schematic representation of the instrument is displayed on Figure 18.

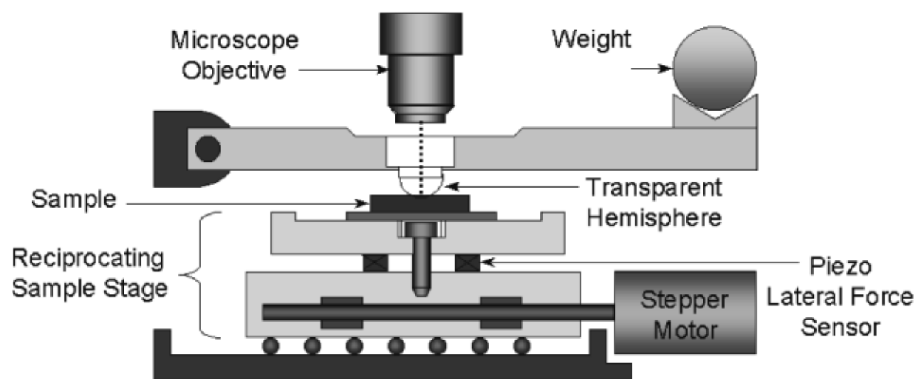


**Figure 17 Raman tribometer (51)**

The picture and composition in addition to the friction measurement can be studied thanks to the microscope objective located above transparent hemisphere.

The instrument is designed for pin on disc tribological tests. Thanks to attached optical microscope, the video and optical imaging as well as Raman spectroscopy can be performed during experiment. For this, transparent hemisphere instead of a steel ball was used in the sample-load contact. This allowed them to study the picture as well as composition of the transfer film (on the hemisphere) in addition to the friction coefficient measurement.

The G-peak intensity of the Raman spectra being directly proportional to the transfer film thickness  $t$ , the data of the Raman spectroscopy could have been likewise used to quantify the transfer film formation (see chapter 2.3 ).

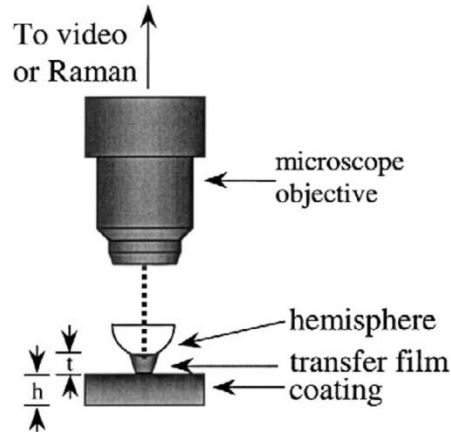


**Figure 18 Observation of the transfer film development**

Transfer film with thickness  $t$ , formed between the hemisphere and a sample coating, was studied (48)

The results of the experiments depict formation, maintenance and finally distortion of the transfer film in the course of circles. Roughly first 400 cycles, as the film was created, thickness exhibited steady growth, Thick transfer film was maintained during 400 – 1400 cycles. Around the cycle 1500 the intensity of the G-peak started to drop back to the value of the coating (starting value), as the transfer film was distorted. Since the transfer firm was no more presented, the cycling of the friction coefficient appeared from around the cycle 1650 on.

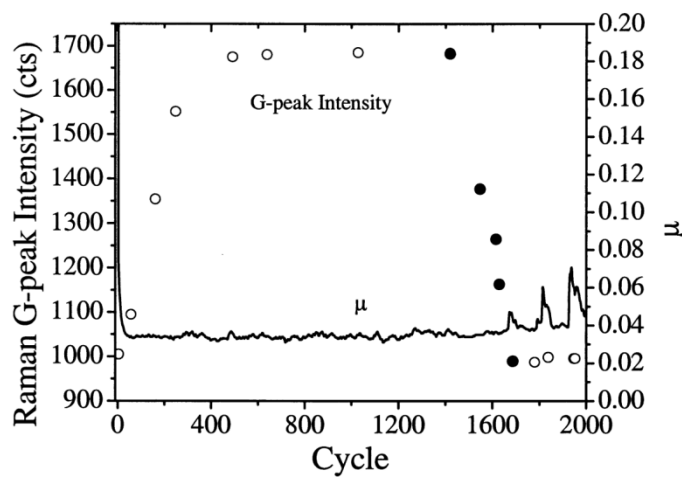


**Figure 19 Formation and distortion of the transfer film**

Transfer film distortion lead to the cycling of the friction coefficient (48)

In our lab the in situ measurements are made with the configuration consisting of homemade camera holder bearing optical cable for the measurement of the Raman spectroscopy attached to tribometer. However the instruments have not been used for the measurements by now, and even by early tests some problems (with the quality of the picture from the camera as well as Raman spectra measurement) occurred. Furthermore the time coordination between the measurements (i.e. synchronizing video, Raman spectra, and friction curve) has to be done.

## **2.2.Instruments description**

The wear process will be studied using the standard instruments such as Pin-on-disk Tribometer, ex-situ Raman Microscope and 3D Optical Surface Profiler. In addition, external optical camera will be attached to the tribometer, allowing the video and optical imaging as well as in-situ Raman spectroscopy measurements during tribological experiments.

The chapter contains only basic description of the instruments, more information can be found on the website of the manufacturer. Focus is not on the principle of function of the devices, as most of them are standardized and widely used in Tribology labs.

In contrary the Raman tribometer consisting of standard CSM tribometer and attached external objective, is explained in more details. The homemade instrument, similar to the one used by Singer (see previous chapter), was introduced to our laboratory only recently.

### **2.2.1. Tribometer**



**Figure 20 CSM Tribometer**

Pin-on-disk tribometer for Friction and Wear characterization

The laboratory is equipped with Pin-on-disk Tribometer from CSM Instruments. The principle of Pin-on-disk Tribometer is explained in chapter 1.1. The tribological tests can be made with samples of a diameter up to 50 mm. The device allows setting of test parameters (speed, frequency, contact pressure, time) and environmental conditions (temperature, humidity and lubricant). The tribometer is controlled by the software InstrumX, which displays friction coefficient and temperature during the experiments and allow us to setup the test parameters.

Load range	up to 60 N
Load resolution	30 mN
Maximum Friction force	10 N
Friction resolution	5 mN
Maximum temperature	1000 °C
Rotation Speed	0.3 - 500 rpm
Maximum test radius	30 mm
Maximum torque	450 mN.m
Stroke length	60 mm
Speed	up to 100 mms <sup>-1</sup>
Frequency	0.1 - 10 Hz

**Table 2 CSM Tribometer Specifications (15)**

### **2.2.2. Profilometer**

Profilometer is an instrument devoted to acquiring surface profile. In the thesis is used 3D Optical Surface Profiler model NewView™ 7000 Series from Zygo. It is based on white light interferometry scanning, being able to quantifying surface roughness with profile heights ranging from < 1 nm up to 20000 µm.

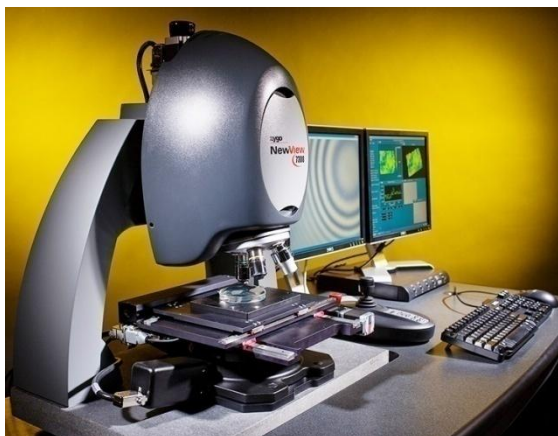


**Figure 21 3D Optical Surface Profiler (52)**

### **2.2.3. Raman Microscope**

Raman spectroscopy gives us information about the molecular composition, chemical bonds and other characteristics of the sample (more information about Raman spectroscopy is given in chapter 3.3.).

In the work, XploRA Raman Microscope with 532 nm laser beam is used. The instrument is connected via optical fiber with the external lens situated above the tribometer.



**Figure 22 XploRA Raman Microscope (53)**

#### 2.2.4. External objective

For the in situ chemical analysis and video recording, the external objective is used. It consists of SuperHead fiber optic probe supplied along with the Raman Microscope by the manufacturer (XploRA) and the homemade stand.



**Figure 23 SuperHead fiber optic probe (45)**

The SuperHead probe is connected to an excitation laser source and base Raman analyzer by fiber optic cable. The color camera allows locating a precise region of interest prior to analysis as well as optical imaging (45).

In contrast to the measurements described in chapter 2.1, the external objective is situated opposite ( $180^\circ$  degrees) to the ball - sample contact. The external probe can thus record the image and other data of the moving sample only with the delay of half period.

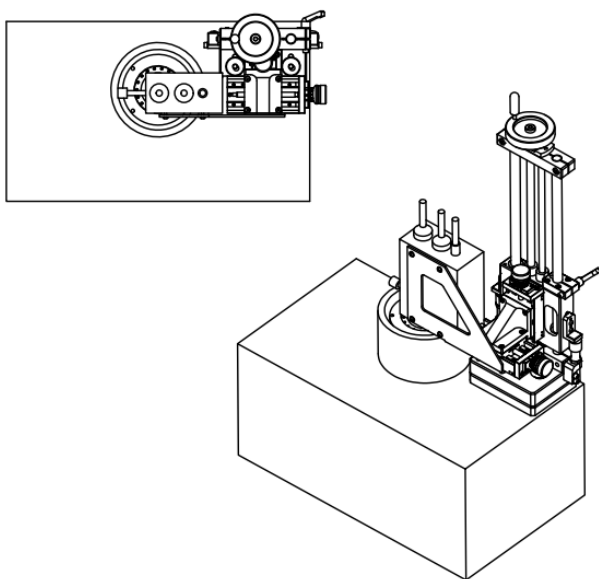


**Figure 24 Stand for SuperHead probe**

The stand allows movement of the probe in all three directions.

The stand was designed according to the requirements of the author's research group. The goal was to allow the probe movement in vertical as well as in horizontal direction. Two small drivers (screws) allow the position control in a horizontal plane, while the vertical movement is made by crank and small driver for a little adjustment.

As the tribometer measurement can be made under different environmental parameters (see chapter 2.2.1), the stand is removable. It is attached to the tribometer with two screws.

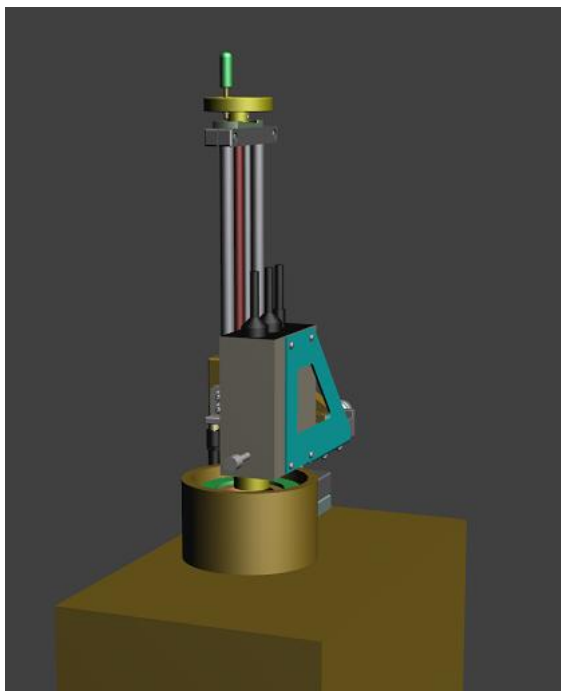


**Figure 25 3d model of the probe stand**

## **2.3.Raman spectroscopy**

Raman spectroscopy is an important nondestructive tool for material identification with little constraints on the substrate size, which helps us to study vibrational, rotational and other low-frequency modes in a system. It relies on inelastic scattering of monochromatic light (46).

When a light quantum  $h\nu_0$  hits a surface, an elastic scattering process (Rayleigh scattering) or an inelastic process (Raman scattering) ensues. By Raman scattering the vibrational energy is altered by  $h\nu_s$  and the emitted photon frequency is shifted. Raman lines corresponding to

emitted photons of energy  $h\nu_0 + h\nu_s$  are called anti-Stokes lines, while those of lower energy ( $h\nu_0 - h\nu_s$ ) are denoted Stokes lines (47).

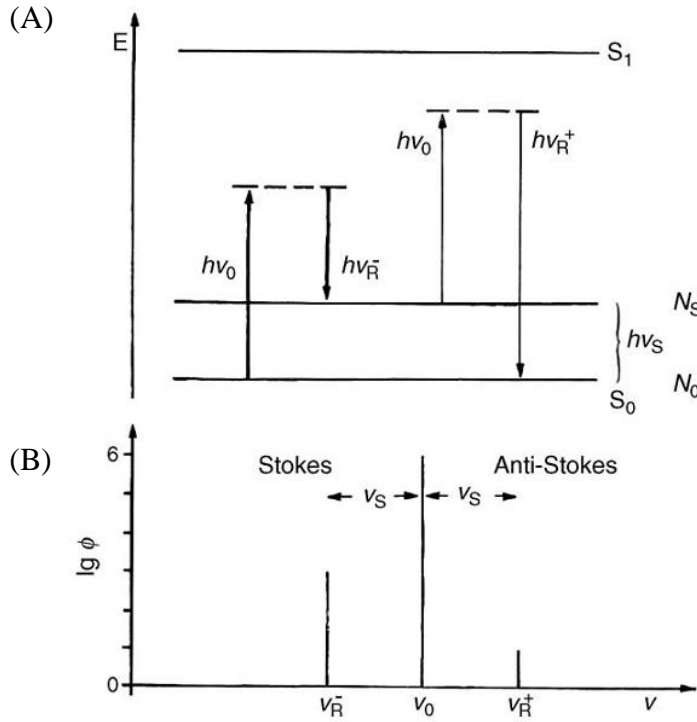


**Figure 26 Raman scattering (45)**  
(A) Energy level diagram (B) Raman spectra

### 2.3.1. Raman spectra interpretation of DLC

The great versatility of carbon materials arises from the strong dependence of their physical properties on the ratio of  $sp^2$  (graphite-like) to  $sp^3$  (diamond-like) Bonds. Diamond Like Carbon is an amorphous carbon with a significant fraction of  $sp^3$  bonds (48).

Raman spectrum of the DLC coating typically shows one peak centered around  $1550\text{cm}^{-1}$ , denoted as G (graphitic), reflecting the zone center  $E_{2g}$  mode of perfect graphite. In a presence of disorder second peak centered at around  $1360\text{ cm}^{-1}$  occurs. It is denoted as D (disorder) and it is more active in transfer films adhered on the surfaces in the contact (48).

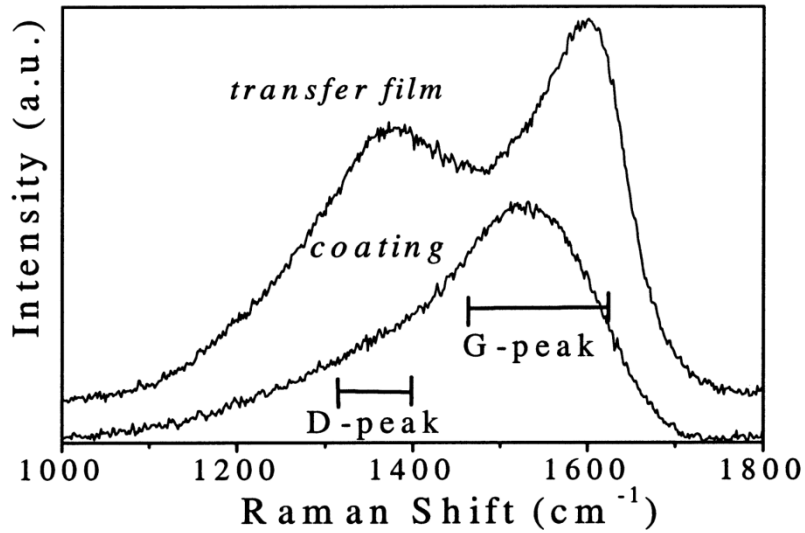


**Figure 27 Raman spectra of DLC**

DLC transfer film Raman spectrum: G (graphitic) and D (disorder) peaks are shown (49).

To reveal more information about the structure of the carbon films, the Raman spectra have to be deconvoluted. The most common Raman spectra fitting method is to employ two Gaussian peaks. Raman spectrum depends on the wave-length of the excitation laser. For evaluation is therefore often used the peak intensity ratio  $I_D/I_G$  or the peak area ration  $A_D/A_G$  respectively (46). They generally vary for DLC films synthesized by different methods and parameters and sometimes even for films fabricated by the same method. However, for the same film, we can often consider them as approximately constant (49).

## 2.4. Raman spectra measurement

As described in chapter 2.2.3 for the in-situ Raman spectra measurement the external objective connected through fiber optic with the Raman Microscope was used. Since the optic fiber decrease laser intensity, we carried out several tests to compare the Raman spectra from Raman microscope with those acquired through the external objective.

### 2.4.1. Raman spectra comparison

The Raman spectra were compared using the reference sample – pure Si provided by manufacturer of the Raman Microscope. The sample was measured repeatedly using the external objective and the data were compared with the Raman Microscope measurement. The laser wavelength was 532 nm; the objective in the Raman Microscope had 100x magnifications, the objective used in the external objective had 5x magnification, and the acquisition time was 60s.

The comparison of intensities obtained from Raman Microscope and external objective was carried out with different laser filters, see Table 3. Intensities measured with filters higher than 25% (on Raman Microscope) and below 1% (on external objective) are not shown as the signal was saturated or unrecognizable from the noise. For both devices (Raman Spectrometer and external objective) two measurements at two different places were made (points A, B, C, and D).

Table 3 shows that the signal from the external objective was approximately 200 times lower than that of standard Raman settings. However, it is clear that the external head can be used to analyze chemical changes in the wear tracks.

laser intensity	Raman Microscope		External objective	
	A	B	C	D
0.1%	570	470		
1.0%	5643	5893	26	28
10.0%	65 000	61 730	250	292
25.0%			652	720
50.0%			1200	1300
100.0%			2120	2300

**Table 3 Raman spectra comparison**

Values not shown were saturated or unrecognizable from the noise.

In situ monitoring of the tribological measurements often requires the optical extension is attached to the SuperHead probe. This extension (see Figure 35 on page 38) is located between the probe and the objective. The extension is 74 mm long with a diameter of 30 mm. We can conclude that extension does not influence observed intensity of Raman signal (Table 4).<sup>1</sup>

<b>laser intensity</b>	<b>Just objective</b>	<b>With the black tube</b>
<b>1.0%</b>	26	55
<b>10.0%</b>	250	278
<b>25.0%</b>	652	646
<b>50.0%</b>	1200	1167
<b>100.0%</b>	2120	2132

**Table 4 Raman measurement with the black tube**

#### **2.4.2. Raman spectra of rotating sample**

After validation of the concept for static measurement, the next step is to identify the possibility to measure Raman spectra of rotating sample. Thus, the Raman spectra of a DLC coating (2µm film thickness) were measured by external probe at different surface-to-probe velocity (i.e. different rotation speed). The spectrum acquisition time was set to 120s; the laser intensities were 10%, 25%, 50%, and 100%. The linear speed was in range 0.05 cms<sup>-1</sup> (lowest achievable speed on the tribometer) to 10 cms<sup>-1</sup>.

The data were fitted with two Gaussian peaks (as described in chapter 2.3.1.). Both the peak intensity ratio  $I_D/I_G$  and the peak area ratio  $A_D/A_G$  were evaluated and compared. As the signal noise was indirectly proportional to laser intensity, the main focus was on full intensity (100%; i.e. no filter applied) data evaluation.

In the first step, the Raman spectra of the DLC sample were measured both with the external probe and directly on the Microscope. The spectra differ significantly. In fact, both the intensity and area ratios were about 0.4 higher (1.75 compared to 1.35 for intensities, 0.75 compared to 0.35 for areas). The shift of the peak positions was not observed.

---

<sup>1</sup> Small variations in intensity are due to different focus, which is set by eye.

Thus, the optical system of external probe influences final spectra. However, it can be corrected using standard spectrum measured directly by Raman spectroscope.

In the second step, the Raman spectra acquired at different sample velocities were compared. As expected, the intensity measured during the rotation was in general lower due to focus; however the spectra were almost identical

The G-peak center position was almost stable and varied from 1562 – 1565, while the positions of the D-peak center varied from 1390 to 1415 (especially for higher velocities). The deconvolution of Raman spectra at different linear speeds contains Appendix 1 .

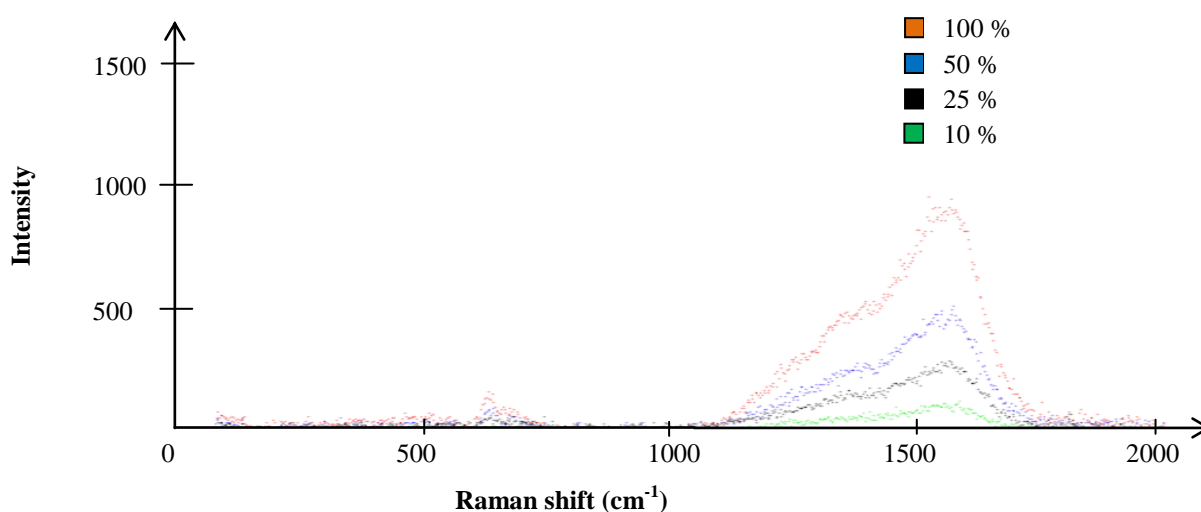


**Figure 28 Raman spectra of the DLC coating**

The measurements were made for different laser intensities (10 % - 100 %)

Figure 29 shows the increase of peak ratio with linear speed when the sample was rotating. However it must be noted that the peak specification was very sensible to the baseline choice. In fact, slight change of the baseline had dramatic effect on the above referred ratio.

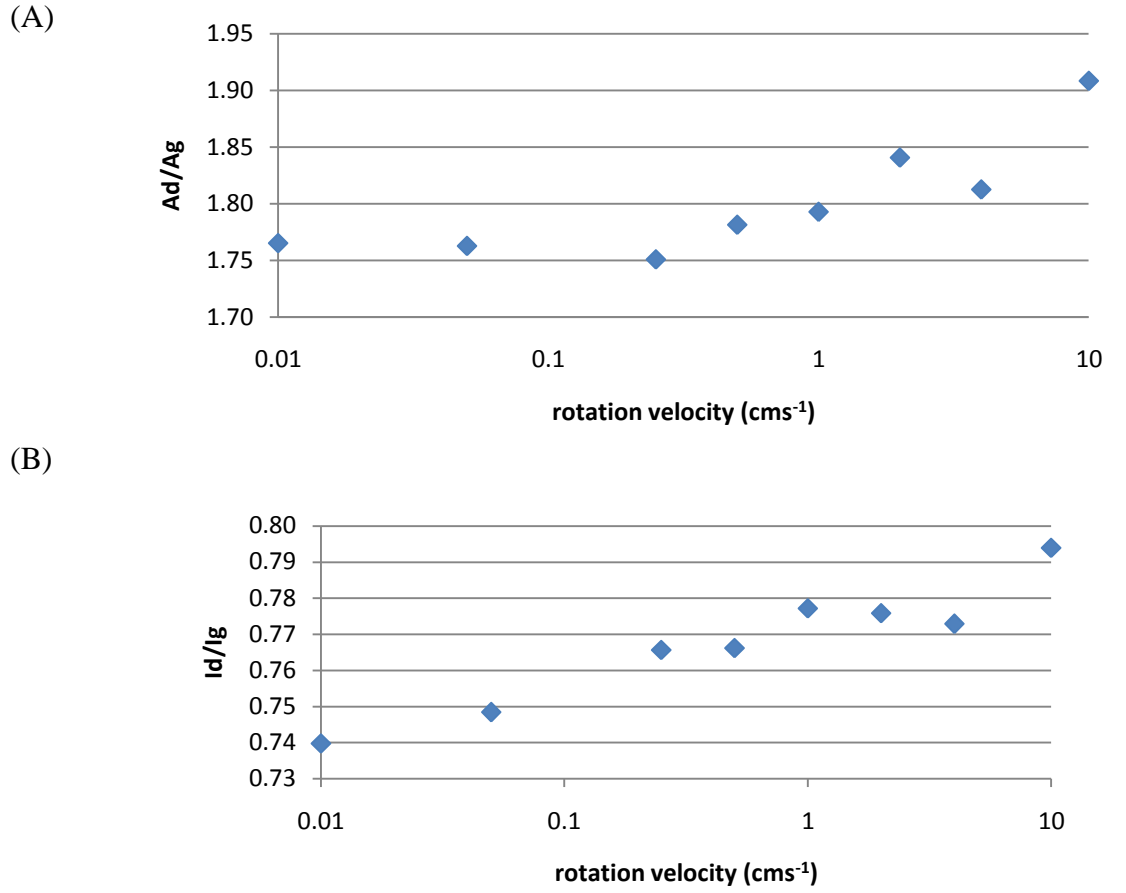


**Figure 29 DLC Raman spectra peak ratios of the moving sample**

(A) ratio of the peak areas (B) ratio of the peak intensities (rotation velocity has logarithmic scale in both plots)

The ratio of the areas was slightly less sensible to rotation than peak intensity ratio. To quantify this, the deviation from the static measurement was calculated by:

$$d = \frac{r_{vx} - r_s}{r_s}, \quad [3]$$

where  $r_s$  is ratio of peak intensities or areas for static measurement and  $r_{vx}$  is ratio at particular speed.

The deviation is expressed in percents and shown in Figure 30.

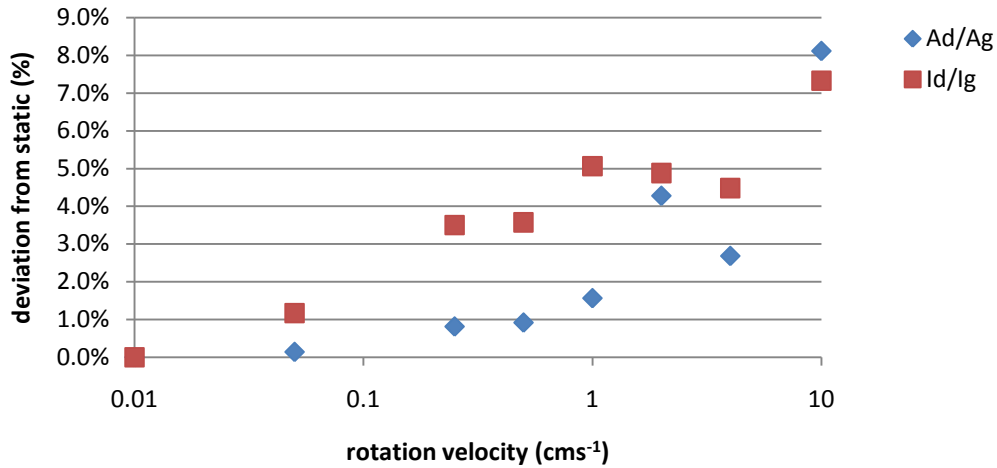


**Figure 30 Deviation of the ratio measurement for different speed of rotation**

Rotation velocity has logarithmic scale.

The deviation of the area ratio was just up to 1% for the rotation velocity  $0.5 \text{ cms}^{-1}$  or lower, while the intensity ratio deviation was almost three times higher. Thus, the linear speed lower than  $0.5 \text{ cms}^{-1}$  is preferred for further analyses.

## 2.5. Video recording optimization

External optical probe can be used as well for optical imaging of the wear tracks. Grabster AV 350 MX is employed to convert the analogue video (S-Video) from the external probe to USB output connected to the computer. The image (or record) is further processed in MAGIX Video TERRATEC Edition application with the maximum frame rate 25 FPS (frames per second).

The position of the external objective records an image of the wear track with a delay of  $\frac{T}{2}$  (half period) after the friction measurement due to setting of the equipment. Therefore, a precise measurement of the sample rotation period is required.

The software InstrumX, which is used to control and monitor the Tribometer (see chapter 2.2.1), can be as well employed for the measurement of friction coefficient as a function of time (typically it is used to measure friction as a function of sliding distance).

The first lap (i.e. period  $T_1$ ), on the InstrumX measurement, often significantly differs from others due to the motor acceleration. Moreover, the cycle period is not measured during

measurement. The exact information about the period length is rarely used in a tribometric data evaluation, as the measurements are often made in a scale of thousands. However it is important to measure the period with high precision (we assume it is not constant, but we call it traditionally as period) in order to correlate the friction coefficient with a video record.

Since the tribometer motor rpm measurement is not precise, we devised an external device that counts the cycles and determines the period based on infrared reflectance sensor. The output of the sensor was compared with video capture using marking on the sample.

### **2.5.1. Sensor design<sup>2</sup>**

Analyzing the requirements of the device and other conditions (such as sample position in tribometer), we decided to apply a sensor measuring the light reflection. The sensor was matched with highly reflective screw attached to the rotating part of the tribometer. The sensor is positioned at exactly 90° from the external objective, on a stand designed according to the sensor's requirements.

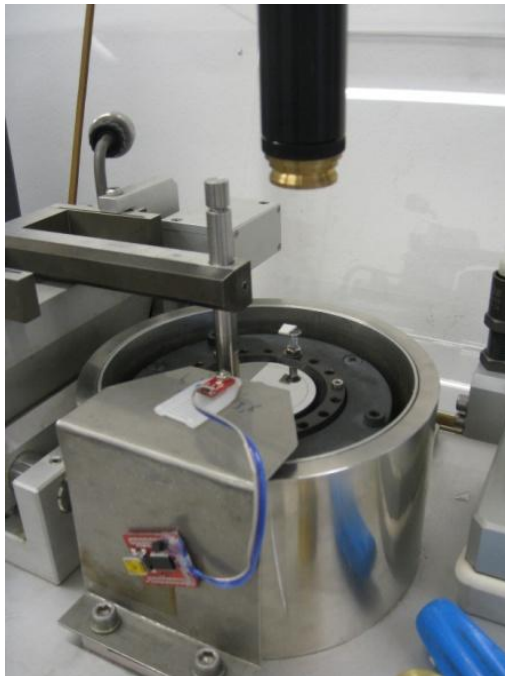


**Figure 31 Sensor on the tribometer**

---

<sup>2</sup> As the author doesn't have experience in the sensor designing and configuration, the developed and implementation was made with a help and support of ing. Zoha

The chosen sensor is *QRE1113 Line Sensor Breakout* and is attached to the board *Breakout Board for FT245RL*, which can be directly connected to the USB port with mini USB connector.

(A)



(B)



**Figure 32 Sensor and Board**

(A) Sensor measuring the amount of reflection (B) Breakout Board

The sensor measures the amount of reflection from the time of discharge: the faster the capacitor discharges, the more reflective the surface is. White surfaces reflect more light than black, so, when directed towards a white surface, the capacitor will discharge faster than it would when pointed towards a black surface (50).

The stand is produced from a stainless steel plate with a thickness of 1mm. It has Z shape and it is attached to the tribometer with two screws on the bottom. The sensor is positioned to match with the reflective screw and is attached to the upper part.

The reflective screw has a white piece of plastic on its *hat* to change the reflectivity and activate the sensor.

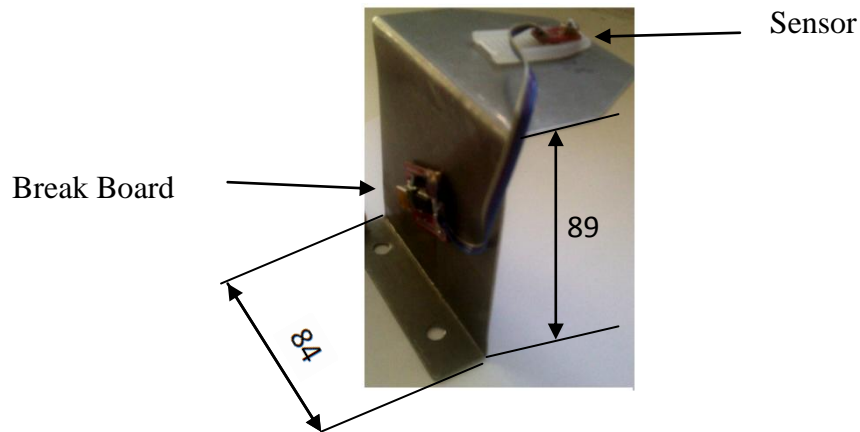


**Figure 33 Sensor on the stand**

To process the data from the sensor, the application was developed in C#. The application communicates with FTD2XX.DLL which contains drivers for the FTDI devices. It is available for download on FTDIchip website (51).

The outputs of the application are: total time, period, and number of cycles as shown in Figure 34. The data are further processed in Excel and Matlab.

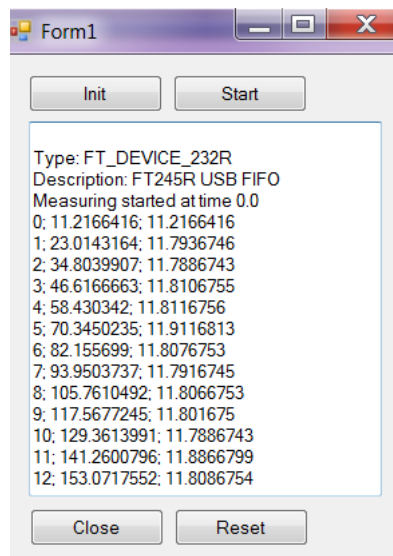


**Figure 34 Application which controls the sensor measurement**

In the three columns are number of cycles, period and total time.

### 2.5.2. Video recording

Correlating a video record with a friction coefficient we have to respect the position of the instruments. As described above, the *pin* (sample-load) contact is positioned  $180^\circ$  from the external objective stand and  $90^\circ$  from the sensor (see Figure 35).

The sensor was programmed to start a measurement when the first event (change of the reflection coefficient) occurs. The highly reflective screw was placed between camera and the pin contact (90 degrees).

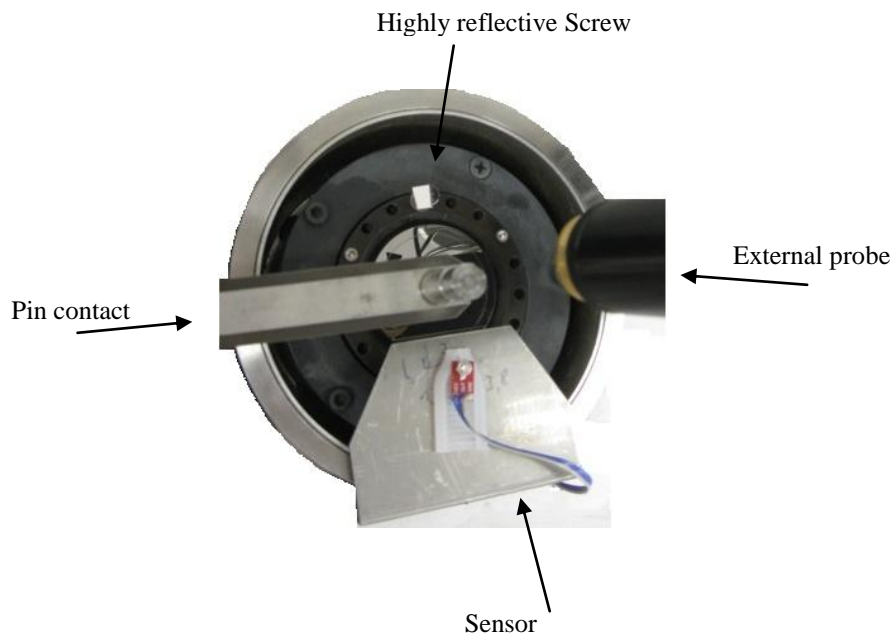


**Figure 35 Instruments arrangement on the tribometer**

### 2.5.3. Testing the tribometer rotation

To test sample rotation, the tribological measurements were carried out using polished steel samples. The test duration was set to 100 laps. The measurements were made with various loads to identify possible correlation between the frictional force (i.e. applied load) and deviation of period.

The standard deviation is expressed in frames, as described in chapter 2.2.4 (the camera has a frame rate 25 frame per second). It means that when it moves with a radius of 2 cm, it makes about 125 frames when moving with the velocity  $2 \text{ cm s}^{-1}$ , but more than 500 frames when moving with the velocity  $0.5 \text{ cm s}^{-1}$ .

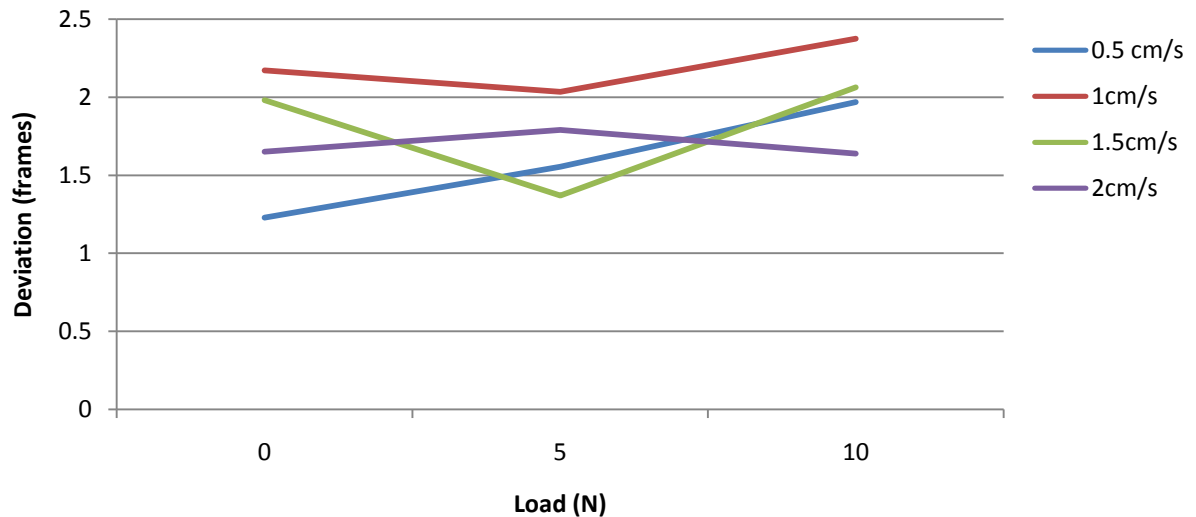


**Figure 36 Deviation of sample rotation.**

As the

Figure 36 shows the rotation period expressed in frames deviates at a rate of about 1 to 2.5 frames per cycle. The deviation from the average was on a both sides (higher and lower values) and didn't accumulate. It cannot be seen any clear dependence on applied weight or rotation velocity.

Better picture gives us the deviation expressed in percents of total frames made by camera in one rotation. Figure 37 shows that, at lower speed, the camera acquires more frames during each rotation which leads to a lower frame deviation.

If the sample rotates with a velocity of  $2 \text{ cm s}^{-1}$ , the object is normally observable only on one frame, but it is on four frames when it moves with a speed  $0.5 \text{ cm s}^{-1}$ .

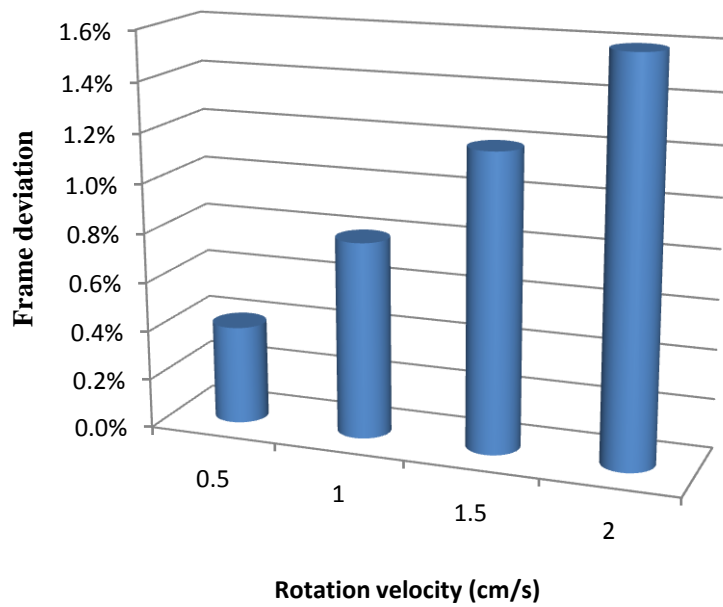


**Figure 37 Deviation of sample rotation in percents**

#### **2.5.4. Initial period**

To associate video with the friction curve, we have to identify the right frame. As referred to above, the initial motor speed might not be constant, so the start of the test would be difficult to relate with optical images. As the device doesn't measure the first half period we have to rely on the average being aware of the velocity limitation (Figure 37).

We carried out sets of measurements to analyze whether initial rotation speed is different from steady state motor regime. Testing steel sample was covered by 4 markings (90 deg).

For selected linear speeds ( $0.5 \text{ cm s}^{-1}$ ,  $1 \text{ cm s}^{-1}$ ,  $1.5 \text{ cm s}^{-1}$ ,  $2 \text{ cm s}^{-1}$ ) we did not observe any difference between the first period and average period from long test. Thus, we can use the average period time calculate from large number of laps to identify the start of the test and thus correlate both measured quantities (friction and images).

## 2.6. Ex-situ wear track profile measurement

The observation of a sample surface is often motivated by detection of an abrupt change of the friction coefficient. The previous chapter described the algorithm for in-situ observation with the external objective. Additional information about the surface can be acquired from ex-situ measurements of the surface using 3D Profilometer (see chapter 2.2.2).

Finding a spot on a surface, which we want to observe  $s_x$ , can be done knowing its exact position relative to known (fixed) point on the surface  $s_0$ . We produce a small black marking on the substrate in order to relate the sample position in 3D profilometer with that of tribometer.

The sample is marked at  $s_0$  and we know the time of friction coefficient measurement of both  $s_x$  and  $s_0$  and the period for given cycle  $p_c$ . We can find spot  $s_0$  on the profilometer. To find the spot  $s_x$ , we first calculate the angular deviation of  $s_x$  by:

$$D_x = \frac{t(s_x) - t(s_0)}{p_c} * 360^\circ, \quad [4]$$

where  $t(s_x)$  and  $t(s_0)$  are times of measurement of  $s_x$  and  $s_0$ .

The position on the sample can be calculated from the trigonometric functions sine and cosine. The approach is not very precise; however it can help us to find the right horizon, in which we might be able to find the spot  $s_x$  comparing the profile measurement with the video record.

### **3. Measurements**

In this section we will suggest an optimum measurement algorithm and the results of testing. The core objective is to synchronize friction coefficient with recorded video and track events by ex-situ observation on 3D profilometer.

#### **3.1. Algorithm of the measurements**

The measurement setup was suggested according to the methodology developed in the last chapter. It summarizes required activities before, during and after the sliding tests. Figure 38 shows an experimental setup. It contains full list of required procedures.

Since March till the submission of the thesis the external probe stopped working. Because of this, the author was able to make the measurements only on steel samples. As the steel does not provide any Raman spectra, all steps containing Raman spectra measurement were skipped. They will be made when the external probe will be repaired.

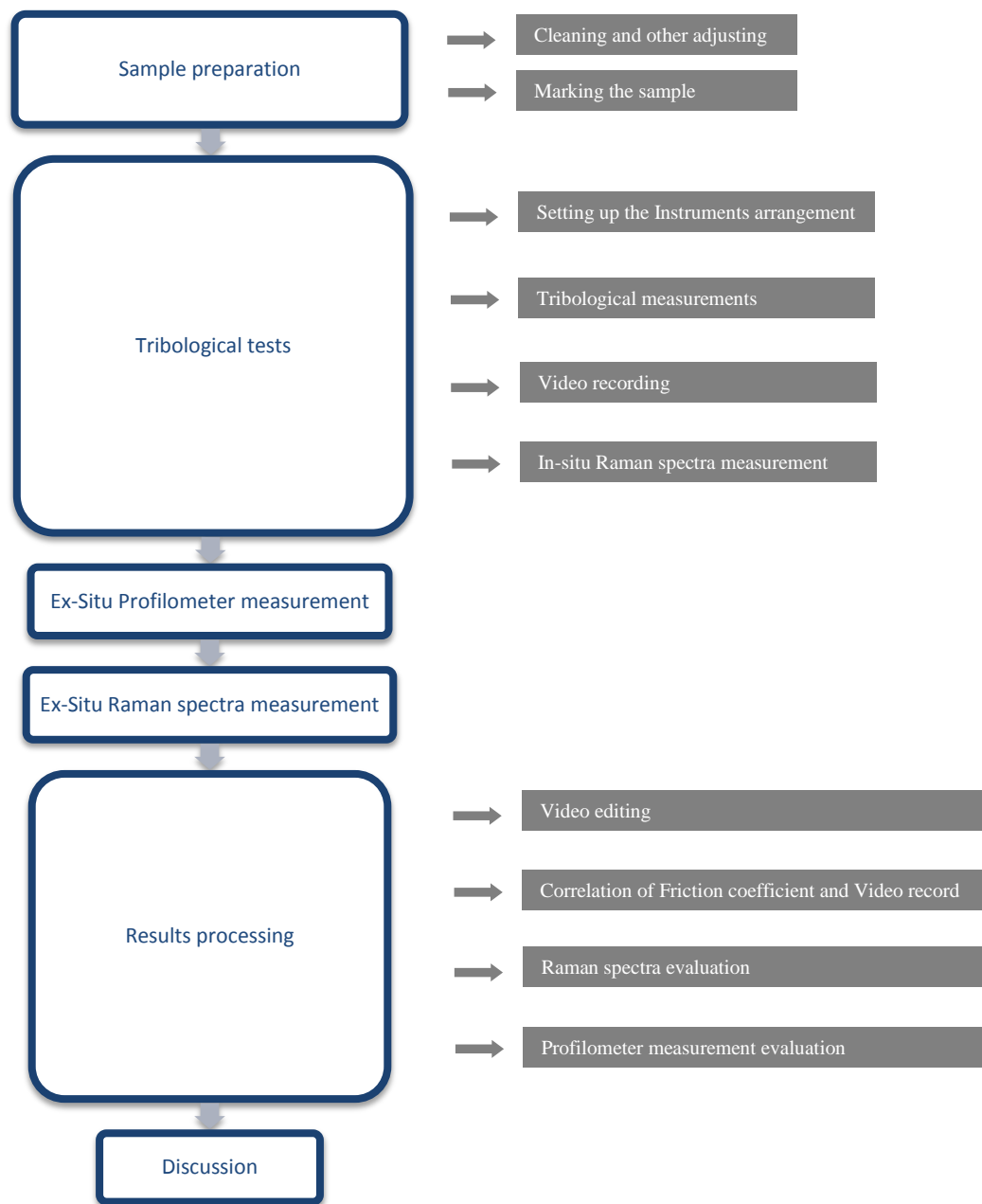


**Figure 38** Algorithm of the measurements

### 3.2. Tribological tests using steel samples

The tests were carried out with steel samples with a diameter of 50 mm; the samples were polished to roughness  $R_a < 30\text{nm}$ , and cleaned using acetone. The main goal of these measurements is to correlate the actual friction coefficient with the video sequence. As described in the chapter 2.6, the author will also testify the possibility of finding the given spot on the sample surface.

Due to the position of external probe (see Figure 35, page 38), the minimal radius of tribological tests is restricted to 14 mm and only one load of 100g (1 N) can be used. To avoid influence of the wear tracks and/or deposition of wear debris into previous track, the wear track should be separated at least 2 mm. The friction partner will be steel ball with a radius of 6 mm. The experiments will be made in ambient temperature. The Acquisition rate was set 10 Hz, linear speed  $1\text{cms}^{-1}$ , the radius 14 mm. The external objective has the magnification 5x.

The measurements are shown on Figure 39 and Figure 40

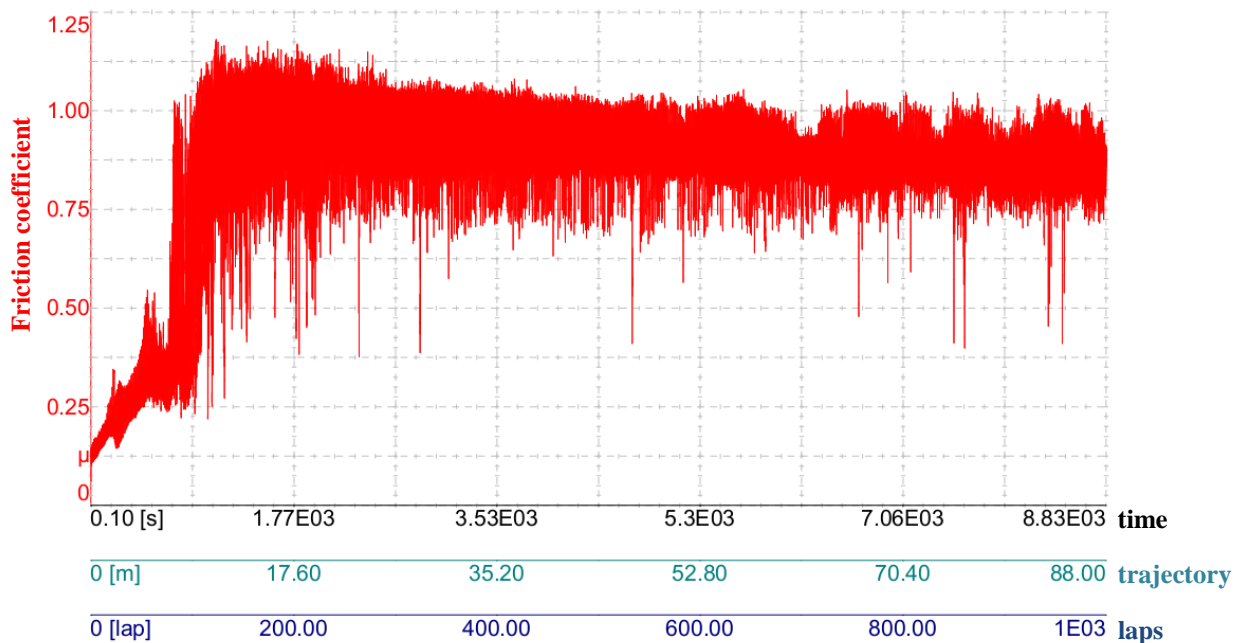
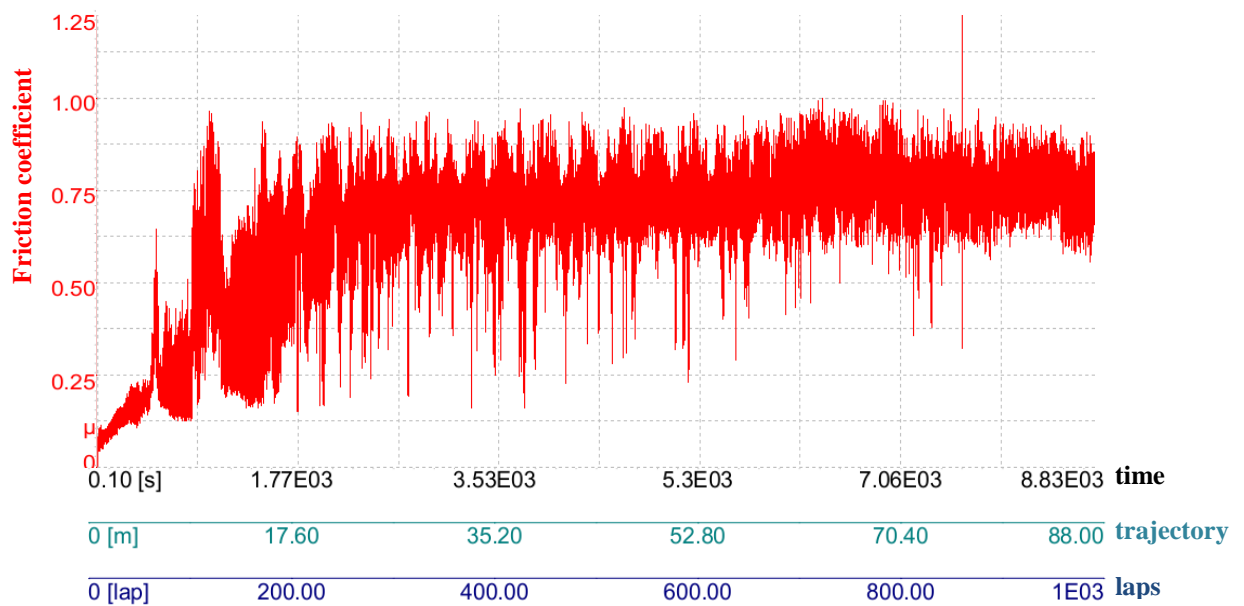


Figure 39 Friction coefficient measurement of a first steel sample

During the first 100 laps, the friction coefficient was gradually growing from less than 0.10 to almost 1.15 (running-in). Then the oscillation of the friction coefficient was lightly decreasing. The reason behind this might be debris from the wear track, which might have served as solid lubricant.

The friction coefficient was periodically oscillating from about 0.70 up to more than 1, with a slow decrease.



**Figure 40 Friction coefficient measurement of a second steel sample**

The wear process on the second steel sample was less stable. However after about 800 laps the friction coefficient started to oscillate around the value 0.7 (from about 0.5 to 0.8). The mean value of the friction coefficient was about 0.2 lower than in the first measurement.

The shape of the friction coefficient oscillation varied significantly during the measurement. As seen on Figure 41, the graphs of the functions are different not only among the measurements but also at different spots of the same measurement. To get the information about this process we have to use in-situ methods as the ex-situ analysis of the worn surfaces is carried out after the test.

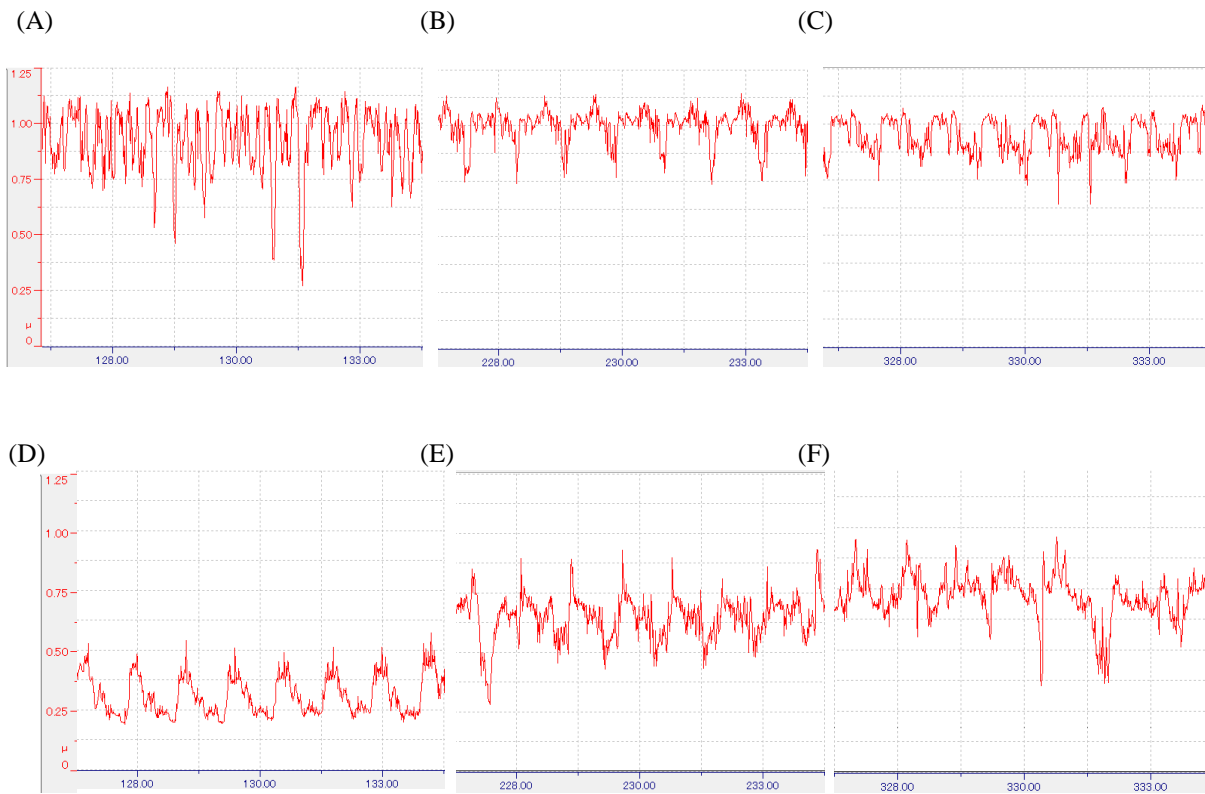


**Figure 41 Friction coefficient oscillation**

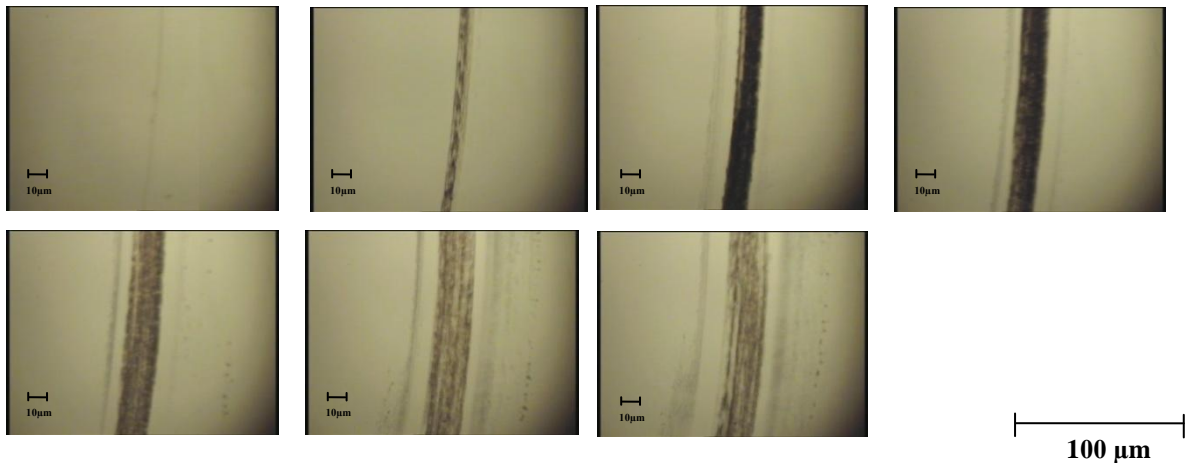
Friction coefficient oscillation changed during the measurements. (A) (D) around 130 laps; (B) (E) around 230 laps; (C)(F) around 330 laps; (A) (B) (C) are from first measurement; (D) (E) (F) are from second measurement

On the camera record we can track the place of maximum (or minimum) friction coefficient, or other spot of interest, throughout the measurement. Wear track development at the spots of the maximum friction coefficient is depicted at Figure 42. The pictures are ordered from the upper left corner to the lower right one.

The measurement of the period used for the picture video record evaluation contains Appendix 2.

The wear track exhibited steady growth. After about 300 laps, the debris from the wear track started to accumulate on both sides of the wear track. The friction coefficient in the first measurement was higher than that of the second test; however the wear track is wider in the later test (as shown on Figure 43). The width of the wear track increased quickly in the first 200 laps, after which it became more stable.

(A)



(B)

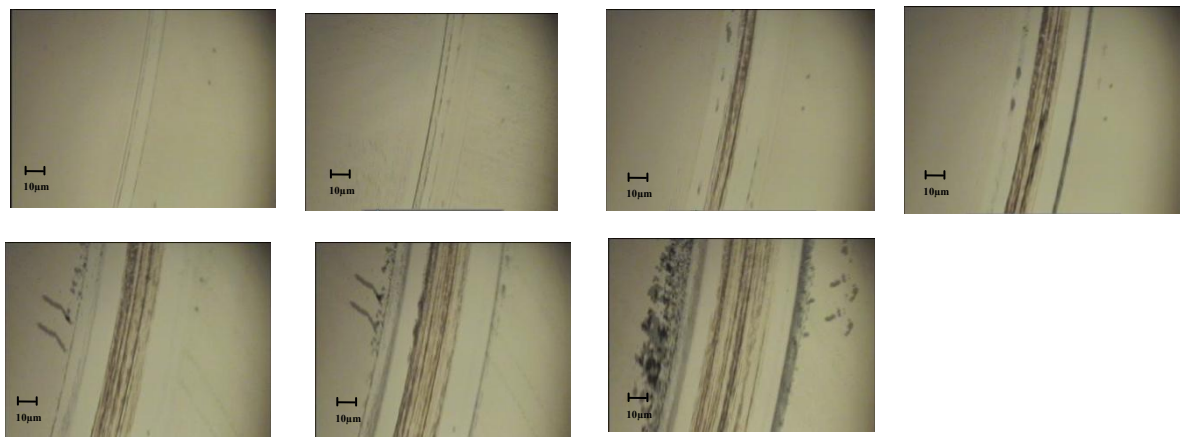


**Figure 42 Wear track development throughout the measurements**

The picture was taken at the spot with maximum friction coefficient after 50, 100, 200, 300, 500, 700 and 1000 laps (from left to right) of (A) first measurement, (B) second measurement.

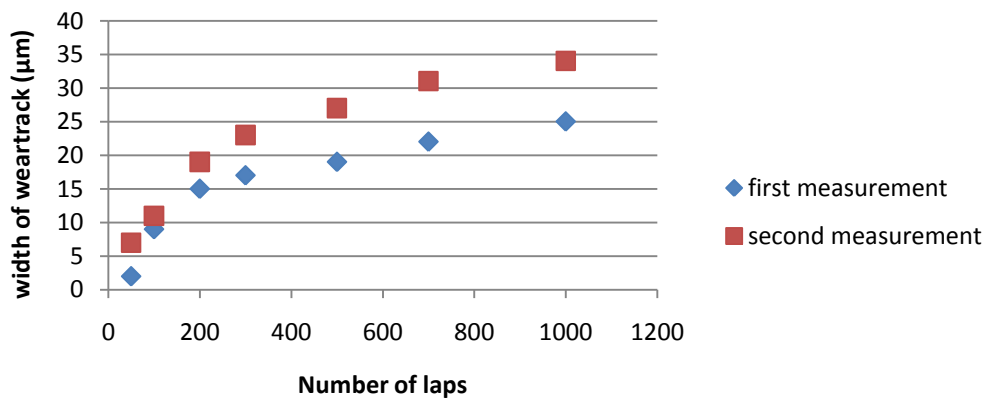


**Figure 43 Growth of the wear track width**

One of the explanations for the higher friction in the first measurement might be the depth of the wear track. For this, the ex-situ profile measurement on Zygo Profilometer was analyzed. The spots in the wear tracks corresponding to the maximum friction of the measurements were compared; average cross-section from three measurements was calculated

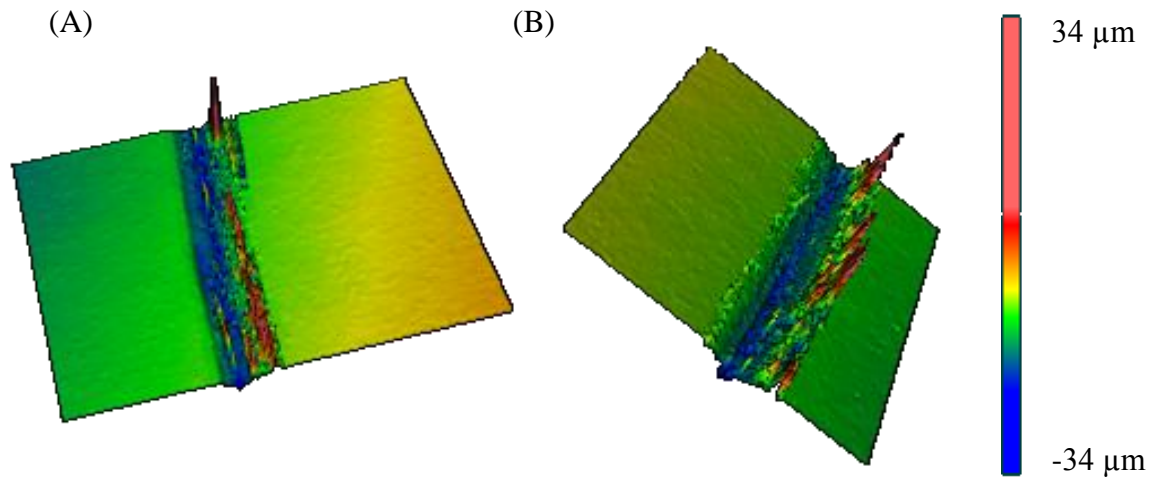


**Figure 44 3d profile of the wear track acquired by Profilometer**

(A) First measurement, (B) Second measurement

The average cross-section of the wear track from the first measurement (at the spot of maximum friction coefficient) was approximately  $19 \mu\text{m}^2$ , while of the second measurement it was just  $13 \mu\text{m}^2$ . The difference of about  $6 \mu\text{m}^2$  might be due to more severe wear at the first measurement. The track is deeper but, as shown on Figure 43, less wide.

### 3.3. Future work

Once the external probe will be repaired the author will finish the in-situ measurements on DLC samples. The goal will be to add the Raman spectra measurements and correlate the resulting peak intensity (or area) ratio with friction coefficient measurement. The similar measurement was made by the author's college Ing. Joao Vitor Pimentel Bernardo, when the external probe was working. The aim of it was analogous to one made by Singer (described in Figure 19 on page 22). The coating observed is WS<sub>2</sub>, which Raman spectra is, similarly to DLC spectra, deconvoluted with two peaks.

On the Figure 45 we can see, that peak intensity developments is slightly correlated with that of friction coefficient.

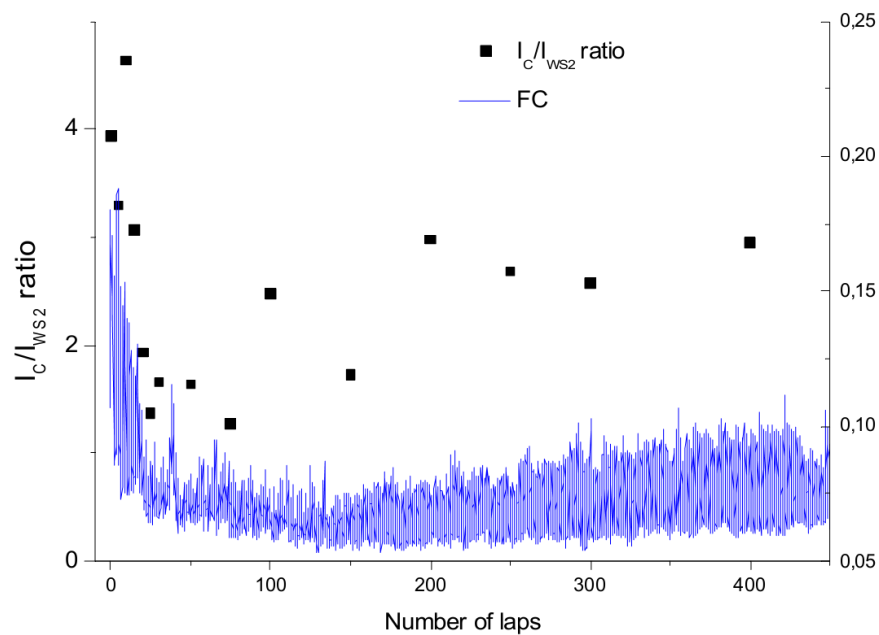


**Figure 45 Raman peak ratios and friction coefficient.**

The measurements of the Raman spectra were made using the external probe; however it was not in-situ measurement. In contrast to the author's intention, ing. Pimentel stopped the test repeatedly during the friction coefficient measurement to make the Raman spectra measurement. Because of this the measurement was not continuous. Moreover, he was not able to measure the change of composition at spots of rapid change of the friction coefficient, such as around 40 laps.

## Conclusion

For the success of space exploration is often critical the durability of moving mechanical components. Effective lubrication can reduce the friction significantly. Diamond-like carbon or DLC with high hardness and low friction is often considered as a potential lubricating material of the future (3).

The main goal of the thesis was to develop the methodology of in-situ optical wear measurement and Raman spectra measurement, and its correlation with friction coefficient measurement. The work has three parts: theoretical, methodological and measurements.

Theoretical part describes the tribology as a science and engineering of interacting surfaces in relative motion. It contains definition and classification of friction, wear and their measurement. One part focuses on lubrication which can effectively lower the friction and wear. Special attention is given to solid lubricants which can be used in extreme conditions of the environment. Diamond Like Carbon as an emerging coating for space industry is described in deeper details in terms of properties and applications.

The design of the methodology is approached in the methodological part. It starts with the description of similar measurements, as the author intends to do, made by Singer. There is also short description of all devices which are later used. Special attention is given to external probe which allow us to make video recording in addition to the Raman spectra measurement. First the author evaluates the possibility of using it for the in-situ Raman spectra measurement at different rotation velocities of the sample. He explains the Raman spectra interpretation of DLC and describes the evaluation technique. It is concluded that the peak area ratio is less sensitive to sample rotation for the velocities lower than  $1 \text{ cm s}^{-1}$ , while the deviation from the static measurement start to grow significantly for velocities higher than that.

The main problem solved in the thesis was to correlate the video record made by the external probe with the friction measurement. For that it is necessary to know the period of the tribometer. Since the tribometer motor rpm measurement is not precise, an external device that counts the cycles and determines the period based on infrared reflectance sensor was designed. Using it the author concludes that the video record deviation is about 2 frames/per cycle (when recorded with the provided camera) and doesn't depend on load and rotation velocity.

The last part of the work demonstrates the proposed methodology. Since the external probe stopped working in March, the author was able to make the measurements only on Steel samples. As they don't provide any Raman spectra, the friction coefficient is correlated only to the video record. It was concluded, that the shape of the friction coefficient oscillation varies significantly not only among the measurements but also at different spots of the same measurement. On the video record was chosen the location of highest friction which was tracked at different spots of the measurement. It was observed, that the width of the wear track increased quickly in the first 200 laps, after which it became more stable. The results of the measurement are compared with the 3D surface metrology, which allows us to compare the resulting width with the average cross-section of the wear track. In the final part of the chapter are described the intentions of the author for the future work once the external probe will be fixed.

## References

1. **Voevodin A., O'Neill J.P., Zabinski J.S.** Nanocomposite tribological coatings for aerospace applications. *Surface and Coatings Technology*. 116, 1999.
2. **Vanhulsel A.** DLC solid lubricant coatings on ball bearings for space applications. *Tribology International*. 40, 2007.
3. **Xiufang L., Liping W.** DLC-based solid–liquid synergetic lubricating coatings for improving tribological. *Wear*. 271, 2011.
4. **Farris, Thomas N.** *Tribology*. Purdue : Purdue University,, 2007. 978-0-444-81764-8.
5. **Czichos, Horst.** *Tribology: a systems approach to the science and technology of friction, lubrication, and wear*. s.l. : Elsevier, 1978. pp. 3, 11-12. 10: 0444416765.
6. **John A. T., Donna M.** Review of solid mechanics in tribology. *International Journal of Solids and Structures*. 37 , 1999., Vols. 1–2.
7. **Holmberg, Kenneth.** Reliability aspects of tribology. *Tribology International*. 34, 2001., Vol. 12.
8. **Yi Qin, Andrew W.** *Micromanufacturing Engineering and Technology*. 2010. p. 221 . 9780815515456.
9. **Grote, Antonsson.** *Springer Handbook of Mechanical Engineering*., s.l. : Springer, 2009. 10: 3540491317.
10. **Persson, B.** *Sliding Friction: Physical Principles and Applications*. s.l. : Springer, 2000. 10: 3540632964.
11. **Kulakowski, Bohdan T.** *Vehicle-Road Interaction*. s.l. : ASTM International, 1994 . 10: 9026515545.

12. **Hirano.** Atomistics of friction. *Surf. Sci. Rep.* 8, 2006, Vol. 60.
13. **Dalmaz, Gérard.** *Transient Processes in Tribology.* s.l. : Elsevier, 2004. 9780444517067.
14. **Godfrey, Douglas.** Friction oscillations with a pin-on-disc tribometer. *Tribology International.* 28, 1993, Vol. 2.
15. CSM TRIBOMETERS. *Nano & Micro range for Tribological studies.* [Online] [Cited: 3 18, 2012.] [http://www.upc.edu/pct/documents\\_equipament/d\\_128\\_id-510.pdf](http://www.upc.edu/pct/documents_equipament/d_128_id-510.pdf).
16. **Mang, Bobzin, Bartels.** *Industrial Tribology: Tribosystems, Wear and Surface Engineering, Lubrication.* s.l. : John Wiley & Sons, 2011. 13: 978- 3527320578.
17. **Stan G, Jane B.** *Engineering Coatings .* s.l. : William Andrew, 1998. 10: 1884207685.
18. **Stachowiak, Batchelor.** *Engineering Tribology, Second Edition .* s.l. : Butterworth-Heinemann, 2000. 10: 0750673044.
19. **Bikramjit B, Mitjan K.** *Tribology of Ceramics and Composites: Materials Science Perspective.* s.l. : John Wiley and Sons, 2011. 10: 0470522631 .
20. **Seliger G, Khraisheh M M. K., Jawahir I. S..** *Advances in Sustainable Manufacturing.* s.l. : Springer, 2011. 1846289343 .
21. **Lakshminarayanan P. A., Nayak N. S..** *Critical Component Wear in Heavy Duty Engines.* s.l. : John Wiley and Sons, 2011 . 10: 0-470-82882.
22. **Stachowiak, Gwidon W.** *Wear: materials, mechanisms and practice.* s.l. : Wiley, 2005. 10: 0470016280.
23. **Roush M. L., Webb W. M..** *Applied Reliability Engineering.* s.l. : RIAC, 2000. 10: 0442004699.

24. **Davis J. R.**, *Surface Engineering for Corrosion and Wear Resistance*. s.l. : ASM International, 2001. 978-1-59124-963-4.
25. **Szeri, Andras Z.** *Fluid Film Lubrication*. s.l. : Cambridge University Press, 2010 . 978052161945.
26. **Dowson, D.** *Lubricants and Lubrication*. Leeds, : Elsevier, 1995.
27. **Shizhu Wen, Ping Huang.** *Principles of Tribology*. s.l. : John Wiley & Sons, 2012. 10-471-59407-5.
28. **Mang T, Dresel W.** *Lubricants and Lubrication*. s.l. : John Wiley & Sons, 2007. 9783527314973.
29. **Pawlak, Zenon.** *Tribochemistry of Lubricating Oils*. s.l. : Elsevier, 2003. 9780444512963.
30. Grease — Its Components and Characteristics. *mobilindustrial*. [Online] 2009. [Cited: 03 29, 2012.] <http://www.mobilindustrial.com/IND/English/Files/tt-components-and-characteristics-of-grease.pdf>.
31. **Bloch, Heinz P.** *Practical Lubrication for Industrial Facilities*. s.l. : The Fairmont Press, 2009. 10: 1420071513.
32. **Rymuza, Zygmunt.** *Tribology of Miniature Systems*. s.l. : Elsevier, 1989. 0444874011 .
33. **Mang T, Dresel W.** *Lubricants and Lubrication*. s.l. : Wiley-VCH, 2007. 9783527314973.
34. **Czichos, Horst.** *Tribology: A Systems Approach to the Science and Technology of Friction, Lubrication, and Wear*. s.l. : Elsevier, 1978. 9780444416766.
35. **Martin J. M, Ohmae N..** *Nanolubricants*. s.l. : John Wiley & Sons, .2008 . 9780470987704.

36. **Erdemir A., Donnet Ch.** Tribology of diamond-like carbon films: recent progress and future prospects. *Journal of Physics D: Applied Physics*. 39 , 2006, Vol. 18.
  
37. **Vižintin, Jože.** *Tribology Of Mechanical Systems: A Guide to Present and Future Technologies*. s.l. : ASME Press, 2004. 9780791802090.
  
38. **Bhushan, Bharat.** *Nanotribology and Nanomechanics: An Introduction*. s.l. : Springer, 2008. 10: 3540242678 .
  
39. **Flege S., Hatada R., Ensinger W., Baba K.** Properties of hydrogenated DLC films as prepared by a combined method of plasma source ion implantation and unbalanced magnetron sputtering. *Journal of Materials Research* /. 27, 2011.
  
40. **Grill, Alfred.** Diamond-like carbon: state of the art. *Diamond and Related Materials*. 8, 1999.
  
41. **Miyake S., Takahashi S., Watanabe I., Yoshihara H.** Friction and wear behavior of hard carbon films. *ASLE Trans*. 30, 1987.
  
42. **Blau P., Steven L. Shaffer.** *15th Wear of Materials*. s.l. : Elsevier, 2005. 9780080447360.
  
43. **Sedlaček M., Podgornik B., Vižintin J.** Tribological properties of DLC coatings and comparison with test results: Development of a database. *Materials Characterization*. 59, 2008, Vol. 2.
  
44. SuperHead Fiber Probes. *HORIBA Jobin Yvon*. [Online] [Cited: 02 25, 2012.]  
<http://www.horiba.com/scientific/products/raman-spectroscopy/raman-systems/qc-process-raman/details/superhead-fiber-probes-150/>.
  
45. **Chu P. K., Liuhe L.** Characterization of amorphous and nanocrystalline carbon films. *Mater. Chem. and Phys*. 2006, Vol. 96, pp. 253-277.

46. **Tuchin, Viktorovich V.** *Tissue optics: light scattering methods and instruments for medical diagnosis*. 2007. p. 645. 0819464333.
47. **Ferrari, Robertson.** Interpretation of Raman spectra of disordered and amorphous carbon. *PHYSICAL REVIEW B*. 61, 2000, Vol. 20.
48. **Scharf, Singer.** Quantification of the Thickness of Carbon Transfer. Films Using Raman Tribometry. *Tribology Letters*. 2003, Vol. 14, pp. 137-145.
49. QRE1113 Line Sensor Breakout - Digital. [Online] [Cited: 3 15, 2012.]  
<http://www.sparkfun.com/products/9454>.
50. ftdichip. [Online] [Cited: 2 15, 2012.]  
<http://www.ftdichip.com/Support/SoftwareExamples/CodeExamples/CSharp.htm>.
51. **Donnet Ch., Erdemir A.** *Tribology of diamond-like carbon films: fundamentals and applications*. s.l. : Springer, 2008. p. 205. 978-0-387- 30264-5.
52. Zygo NewView™ 7000 Series. *3D Optical Surface Profilers*. [Online] [Cited: 02 25, 2012.] <http://www.zygo.com/?/met/profilers/newview7000/>.
53. XploRA Raman Microscope. *HORIBA Jobin Yvon*. [Online] [Cited: 02 25, 2012.]  
<http://www.horiba.com/fileadmin/uploads/Scientific/Documents/Raman/xplora.pdf>.
54. **Dresselhuys D. M., Klok H. J.** Tribology of o/w Emulsions Under Mouth-like Conditions:. *Food Biophysics*. 2, 2007.
55. **Bremond F., Fournier P.** Test temperature effect on the tribological behavior of DLC-coated 100C6-steel couples in dry friction. *Wear*. 254, 2003, Vols. 7–8.
56. **Mang T., Dresel W.** *Lubricants and Lubrication*. s.l. : Wiley-VCH, .2007.
57. **Donnet C., Grill A.** Friction control of diamond-like carbon coatings. *Surf. Coat. Technol.* 94–95, 1997.

58. **Hwanga D.H., Gahr K.H.** Transition from static to kinetic friction of unlubricated or oil lubricated steel/steel, steel/ceramic and ceramic/ceramic pairs. *Wear* . 255, 2003, Vols. 1–6.
59. **Masjuki H.H., Maleque M.A.** Investigation of the anti-wear characteristics of palm oil methyl ester using a four-ball tribometer test. *Wear*. 206, 1997, Vols. 1–2.

## Tables

Table 1 Comparison of mechanical properties of DLC with various carbon materials .....	18
Table 2 CSM Tribometer Specifications .....	24
Table 3 Raman spectra comparison.....	30
Table 4 Raman measurement with the black tube .....	31

## Figures

Figure 1 Types of friction .....	6
Figure 2 Tribometer .....	7
Figure 3 Example of ball on plate tribometer.....	8
Figure 4 Four-ball tribometer .....	8
Figure 5 Mechanism of Adhesion .....	9
Figure 6 Mechanism of Abrasive wear .....	10
Figure 7 Modes of Abrasive wear .....	11
Figure 8 States of friction .....	12
Figure 9 Principle of hydrodynamic lubrication.....	13
Figure 10 Stribeck curve (simplified).....	13
Figure 11 Friction reduction by soft metal film .....	15
Figure 12 Lubrication by lamellar solids .....	16
Figure 13 Structure of graphite .....	16
Figure 14 Hardness and friction characteristics of DLC .....	17
Figure 15 Phase diagram of the DLC .....	17
Figure 16 Influence of temperature on friction coefficient .....	19
Figure 17 Raman tribometer .....	21
Figure 18 Observation of the transfer film development.....	22
Figure 19 Formation and distortion of the transfer film .....	22
Figure 20 CSM Tribometer .....	23
Figure 21 3D Optical Surface Profiler .....	25
Figure 22 XploRA Raman Microscope .....	25
Figure 23 SuperHead fiber optic probe .....	26

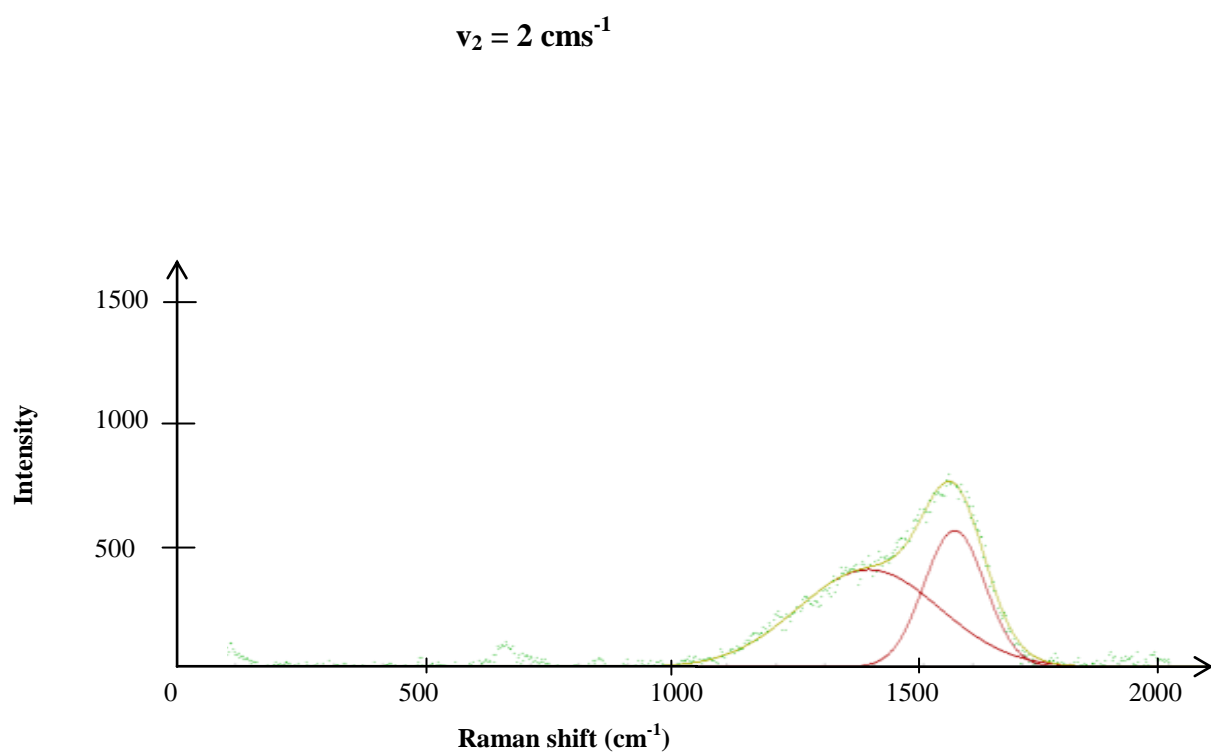
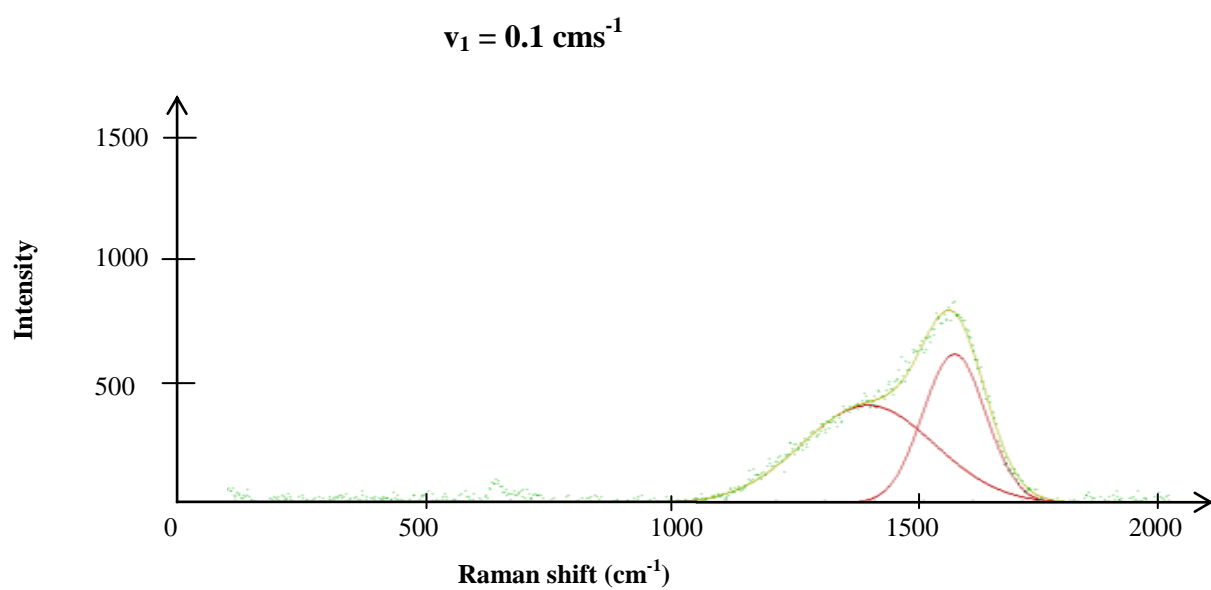
Figure 24 Stand for SuperHead probe .....	26
Figure 25 3d model of the probe stand .....	27
Figure 26 Raman scattering .....	28
Figure 27 Raman spectra of DLC .....	29
Figure 28 Raman spectra of the DLC coating .....	32
Figure 29 DLC Raman spectra peak ratios of the moving sample .....	33
Figure 30 Deviation of the ratio measurement for different speed of rotation.....	34
Figure 31 Sensor on the tribometer .....	35
Figure 32 Sensor and Board .....	36
Figure 34 Application which controls the sensor measurement.....	37
Figure 33 Sensor on the stand .....	37
Figure 35 Instruments arrangement on the tribometer .....	38
Figure 36 Deviation of sample rotation.....	39
Figure 37 Deviation of sample rotation in percents .....	40
Figure 38 Algorithm of the measurements .....	43
Figure 39 Friction coefficient measurement of a first steel sample .....	44
Figure 40 Friction coefficient measurement of a second steel sample .....	45
Figure 41 Friction coefficient oscillation.....	46
Figure 43 Growth of the wear track width .....	47
Figure 42 Wear track development throughout the measurements.....	47
Figure 44 3d profile of the wear track acquired by Profilometer.....	48
Figure 45 Raman peak ratios and friction coefficient. ....	49

## **List of Appendices**

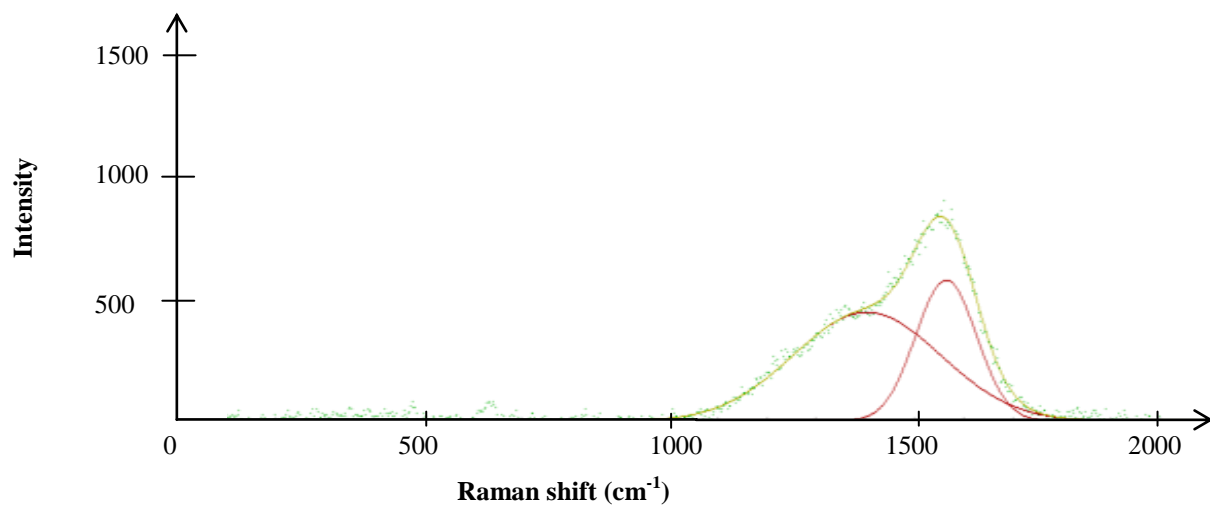
**Appendix 1: Deconvolution of Raman spectra at different linear speed**

**Appendix 2: Measurement of period**

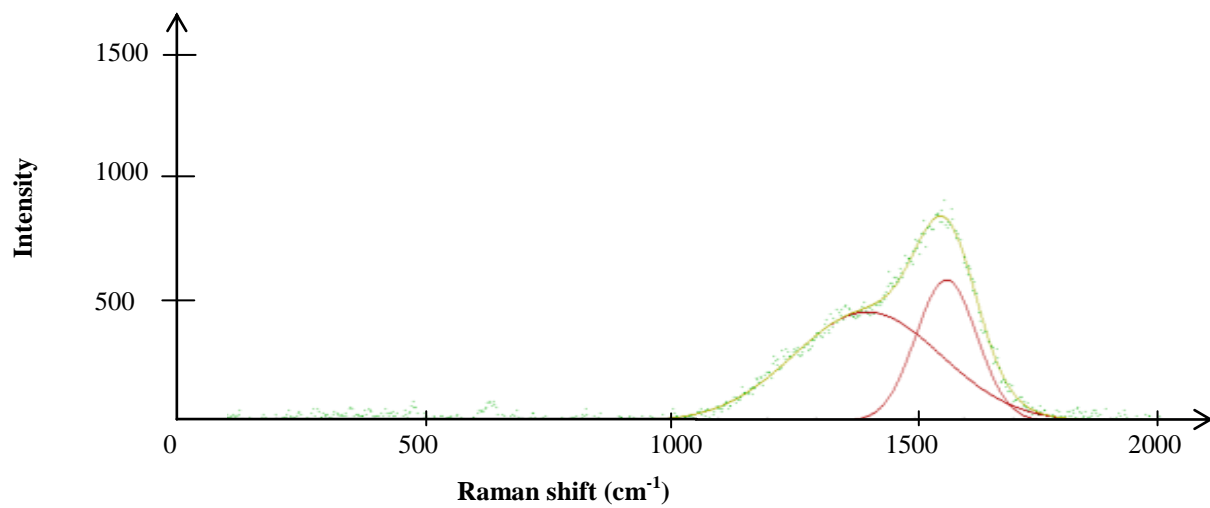
## Appendix 1: Deconvolution of Raman spectra at different linear speed



$$\nu_3 = 4 \text{ cm s}^{-1}$$



$$\nu_4 = 10 \text{ cm s}^{-1}$$



## Appendix 2: Measurement of period of the first measurement

First 50 laps :

Cycle	total time (s)	period (s)
1	9.062518	9.062518
2	17.909024	8.846506
3	26.748530	8.839506
4	35.716043	8.967513
5	44.545548	8.829505
6	53.612067	9.066519
7	62.454572	8.842506
8	71.396084	8.941511
9	80.350596	8.954512
10	89.089096	8.738500
11	98.145614	9.056518
12	106.984119	8.838506
13	115.825625	8.841506
14	124.885143	9.059518
15	133.725649	8.840506
16	142.587155	8.861507
17	151.532667	8.945512
18	160.378173	8.845506
19	169.442691	9.064518
20	178.389203	8.946512
21	187.121703	8.732500
22	196.188221	9.066519
23	205.030727	8.842506
24	213.872232	8.841506
25	222.931751	9.059518
26	231.787257	8.855507
27	240.682766	8.895509
28	249.523272	8.840506
29	258.467783	8.944512
30	267.532302	9.064519
31	276.314804	8.782502
32	285.185311	8.870507
33	294.173825	8.988514
34	303.108336	8.934511
35	311.948842	8.840506
36	320.929356	8.980514
37	329.895869	8.966513
38	338.752375	8.856507
39	347.632883	8.880508
40	356.688401	9.055518
41	365.526907	8.838506
42	374.369412	8.842506
43	383.423930	9.054518
44	392.380443	8.956512
45	401.124943	8.744500
46	410.195462	9.070519
47	419.054968	8.859507
48	428.033482	8.978514
49	436.788983	8.755501
50	445.804498	9.015516

Average period from the whole measurement:

$$T_A = 8.927747 \text{ s}$$

Standard deviation

$$\sigma = 0.094602 \text{ s}$$